



HAL
open science

Metallicity of M dwarfs. IV. A high-precision [Fe/H] and Teff technique from high-resolution optical spectra for M dwarfs

V. Neves, X. Bonfils, N. C. Santos, X. Delfosse, T. Forveille, F. Allard, S. Udry

► **To cite this version:**

V. Neves, X. Bonfils, N. C. Santos, X. Delfosse, T. Forveille, et al.. Metallicity of M dwarfs. IV. A high-precision [Fe/H] and Teff technique from high-resolution optical spectra for M dwarfs. *Astronomy and Astrophysics - A&A*, 2014, 568, 10.1051/0004-6361/201424139 . insu-03618548

HAL Id: insu-03618548

<https://insu.hal.science/insu-03618548>

Submitted on 24 Mar 2022

HAL is a multi-disciplinary open access archive for the deposit and dissemination of scientific research documents, whether they are published or not. The documents may come from teaching and research institutions in France or abroad, or from public or private research centers.

L'archive ouverte pluridisciplinaire **HAL**, est destinée au dépôt et à la diffusion de documents scientifiques de niveau recherche, publiés ou non, émanant des établissements d'enseignement et de recherche français ou étrangers, des laboratoires publics ou privés.



Distributed under a Creative Commons Attribution 4.0 International License

Metallicity of M dwarfs

IV. A high-precision [Fe/H] and T_{eff} technique from high-resolution optical spectra for M dwarfs $\star, \star\star, \star\star\star$

V. Neves^{1,2,3}, X. Bonfils^{3,4}, N. C. Santos², X. Delfosse^{3,4}, T. Forveille^{3,4}, F. Allard⁵, and S. Udry⁶

¹ Departamento de Física, Universidade Federal do Rio Grande do Norte, 59072-970 Natal, RN, Brazil
email: vasco.neves@dfte.ufrn.br

² Centro de Astrofísica and Faculdade de Ciências, Universidade do Porto, Rua das Estrelas, 4150-762 Porto, Portugal

³ Univ. Grenoble Alpes, IPAG, 38000 Grenoble, France

⁴ CNRS, IPAG, 38000 Grenoble, France

⁵ Centre de Recherche Astrophysique de Lyon, UMR 5574: CNRS, Université de Lyon, École Normale Supérieure de Lyon, 46 allée d'Italie, 69364 Lyon Cedex 07, France

⁶ Observatoire de Genève, Université de Genève, 51 chemin des Maillettes, 1290 Sauverny, Switzerland

Received 6 May 2014 / Accepted 23 June 2014

ABSTRACT

Aims. In this work we develop a technique to obtain high precision determinations of both metallicity and effective temperature of M dwarfs in the optical.

Methods. A new method is presented that makes use of the information of 4104 lines in the 530–690 nm spectral region. It consists in the measurement of pseudo equivalent widths and their correlation with established scales of [Fe/H] and T_{eff} .

Results. Our technique achieves a rms of 0.08 ± 0.01 for [Fe/H], 91 ± 13 K for T_{eff} , and is valid in the $(-0.85, 0.26$ dex), (2800, 4100 K), and (M0.0, M5.0) intervals for [Fe/H], T_{eff} and spectral type respectively. We also calculated the RMSE_V which estimates uncertainties of the order of 0.12 dex for the metallicity and of 293 K for the effective temperature. The technique has an activity limit and should only be used for stars with $\log L_{\text{H}\alpha}/L_{\text{bol}} < -4.0$.

Key words. stars: atmospheres – stars: fundamental parameters – stars: late-type – stars: low-mass – methods: data analysis

1. Introduction

The precise derivation of M dwarf atmospheric parameters is still very challenging today. Cool and intrinsically faint, M dwarfs are not easy to study. As the M subtype increases more molecules form in their atmosphere, making the spectral continuum very hard or impossible to identify, at least in the visible region of the spectrum. Therefore, methods such as atomic line analysis that are dependent on the knowledge of the continuum are suited only for the metal poor and earliest types of M dwarfs (e.g. Woolf & Wallerstein 2005, 2006). On the other hand, spectral synthesis techniques do not reach yet a high precision comparable to FGK dwarf methods, due to the fundamental lack of knowledge of billions of molecular line strengths and transitions, and most studies have reached modest results (e.g. Valenti et al. 1998; Bean et al. 2006). Despite that, some important progress have been made using spectral synthesis fitting to high-resolution spectra in the infrared (Önehag et al. 2012), where the depression of the continuum in some regions is less intense than in the visible region of the spectrum (e.g. Rajpurohit et al. 2013b). However, only a few stars have been measured this

way, and the technique lacks external confirmation. An alternative method, based on high-resolution template spectra, to calculate metallicity, distance, stellar mass, and radius, was presented by Pineda et al. (2013). This new technique, with similarities with our own method (Neves et al. 2013), is very promising but its [Fe/H] precision is still limited to 0.15 dex.

In this context, most parameter determinations, especially metallicity and effective temperature are instead based on calibrations using colours (e.g. Bonfils et al. 2005; Johnson & Apps 2009; Schlafman & Laughlin 2010; Johnson et al. 2012; Neves et al. 2012) or spectroscopic indices (e.g. Rojas-Ayala et al. 2010, 2012; Mann et al. 2013a,b; Newton 2013).

Regarding metallicity, some progress has been made in the last few years. A steady improvement was achieved, bringing the typical uncertainties of ± 0.20 dex of the photometric calibrations, below ~ 0.10 dex in the most recent low-resolution spectroscopic scales in the infrared (e.g. Rojas-Ayala et al. 2012; Mann et al. 2013a; Newton 2013), following the pioneering work of Rojas-Ayala et al. (2010). However a true high-precision determination with a rms of the order of 0.05 dex, on par with the ones obtained for FGK dwarfs (e.g. Santos et al. 2004; Sousa et al. 2007) has not yet been reached (see Neves et al. 2012 introduction).

For temperature, on the other hand, important uncertainties and systematics still persist today. Although internal precisions are reported to be lower than 100 K (e.g. Casagrande et al. 2008; Rojas-Ayala et al. 2012; Boyajian et al. 2012), their suffer from systematics ranging from 150 to 300 K making the

* Based on observations made with the HARPS instrument on the ESO 3.6 m telescope at La Silla Observatory under programme ID 072.C-0488(E)

** Our method is available online at <http://www.astro.up.pt/resources/mcal>

*** Tables 1, 2, 4, 8 are available in electronic form at <http://www.aanda.org>

determination of accurate temperature for M dwarfs a priority. In this context [Boyajian et al. \(2012\)](#) presented several calibrations of T_{eff} , based on the largest sample to date of high precision interferometric measurements of K and M dwarf radii and bolometric fluxes, that in principle allow a very precise measurement of the effective temperature (a technique pioneered by [Ségransan et al. 2003](#), for M dwarfs). However, some doubts still arise regarding the accuracy of the determination of the total flux of the stars, based on templates from [Pickles \(1998\)](#), as recently pointed out by [Mann et al. \(2013b\)](#). They have, in turn, also recently presented their own effective temperature method that is very similar to the one of [Boyajian et al. \(2012\)](#) but rely on a combination of their low resolution spectra with BT-SETTL synthetic spectra from [Allard et al. \(2011, 2013\)](#) to calculate the bolometric flux. From these high-precision effective temperatures they established four visual and infrared spectroscopic indices, with precisions (but not accuracies) between 62 and 100 K. A similar effort regarding T_{eff} determination of M dwarfs using synthetic spectra came from [Rajpurohit et al. \(2013a\)](#), where they compare synthetic spectra from the latest BT-SETTL models ([Allard et al. 2012](#)) to low-resolution optical spectra. They obtain a better agreement between synthetic and observed spectra when compared with previous models, estimating uncertainties of T_{eff} of the order of 100 K.

In this work we present a new method to try to overcome the aforementioned hurdles and improve on the precision of both metallicity and effective temperature of M dwarfs. An early version of this new technique was briefly presented in the Appendix of [Neves et al. \(2013\)](#) and used to investigate the planet-metallicity relation of the HARPS GTO M dwarf sample ([Bonfils et al. 2013](#)). In Sect. 2 we describe in detail our method, as well as the sample selection, uncertainty estimation and a test of the technique as a function of resolution and signal-to-noise ratio (S/N). Afterwards, in Sect. 3, we compare our results with other determinations from the literature. Finally, in Sect. 4 we discuss our results. The instructions to use our method are described in the Appendix.

2. The method

Our new method is based on the measurement of pseudo equivalent widths (EWs) of most lines/features in the 530–690 nm region of the spectra from a 102 star sample from the HARPS GTO M dwarf program, described in detail in Sect. 2 of [Bonfils et al. \(2013\)](#). It is a volume-limited sample (11 pc), and contains stars with $\delta < +20^\circ$, $V < 14$ mag and includes only targets with $v \sin i \leq 6.5 \text{ km s}^{-1}$. Spectroscopic binaries as well as visual pairs with separations lower than $5''$ were removed a priori.

The features are defined as regions of the spectra that are formed by more than one line. The EWs are then correlated with the reference photometric [Fe/H] and T_{eff} scales from [Neves et al. \(2012\)](#) and [Casagrande et al. \(2008\)](#) respectively. The two scales are in turn based on [Fe/H] determinations from FGK primaries with a M dwarf secondary and on an adaptation of the IRFM technique ([Blackwell & Shallis 1977](#)) respectively.

This method achieves an increase in precision of both parameters whereas its accuracy is tied to the original calibrations. The methodology is detailed in Sect. 2.1.

The reference [Fe/H] was calculated using stellar parallaxes, V , and K_S magnitudes following the procedure described in [Neves et al. \(2012\)](#). The reference T_{eff} is the average value of the $V - J$, $V - H$, and $V - K$ photometric scales taken from [Casagrande et al. \(2008\)](#). Table 1 lists the quantities used to calculate these parameters. Column 1 shows the star name, Cols. 2

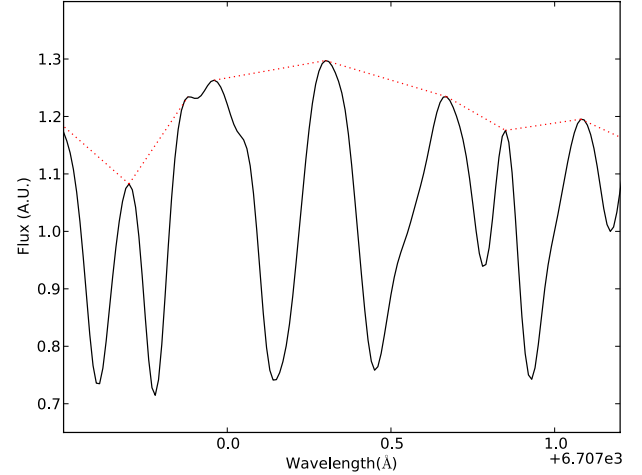


Fig. 1. Small region of the GJ 205 spectra illustrating pseudo equivalent width line measurement. The red dotted line represents the “peak-to-peak” flux.

and 3 the right ascension and declination respectively, Col. 4 the parallax of each star and its associated error, and Col. 5 the source of the parallax measurement. Column 6 depicts the stellar type of the star taken from Simbad¹ ([Wenger et al. 2000](#)), except in the case of GJ438, where it was obtained from [Hawley et al. \(1997\)](#). The photometric stellar type presented in Col. 7 was calculated with the colour relation of [Lépine et al. \(2013\)](#), and Cols. 8 to 11 display the V , J , H , and K_S photometry. Lastly, Col. 12 details the source of the photometry.

From the 110 stars of our sample we first selected 69 stars with spectra having a signal to noise higher than 100. The final spectrum of each star was constructed from median normalised individual observations. The S/N of the individual spectra were added in quadrature. Our final sample is determined by an activity cut, as detailed in Sect. 2.2.

2.1. Method

From our final sample we measured pseudo EWs of lines and features (blended lines) from the spectra in the region between 530 and 690 nm, but excluded the features from the regions between 588–590.5, 656.1–656.4, and 686–690 nm due to the location of the activity sensitive Na doublet and $H\alpha$ lines, and the heavy presence of telluric lines respectively. We define the pseudo EWs as

$$W = \sum \frac{F_{pp} - F_\lambda}{F_{pp}} \Delta\lambda, \quad (1)$$

where F_{pp} is the value of the flux between the peaks of the line/feature at each integration step and F_λ the flux of the line/feature. The measurements of the EWs are illustrated in Fig. 1, where the “peak-to-peak” flux corresponds to the red dotted lines and the flux of the star is shown as a black line.

The very high S/N spectrum of the star GJ205 was used as a reference to establish the line/feature regions that were going to be measured in all spectra. We rejected all lines/features with a EW lower than 8 mÅ to ensure that all lines in stars with lower [Fe/H] or/and T_{eff} can be properly measured. Lines with steep slopes are usually joined with adjacent lines, and measured as one feature. At the end of the line selection we

¹ <http://simbad.u-strasbg.fr/>

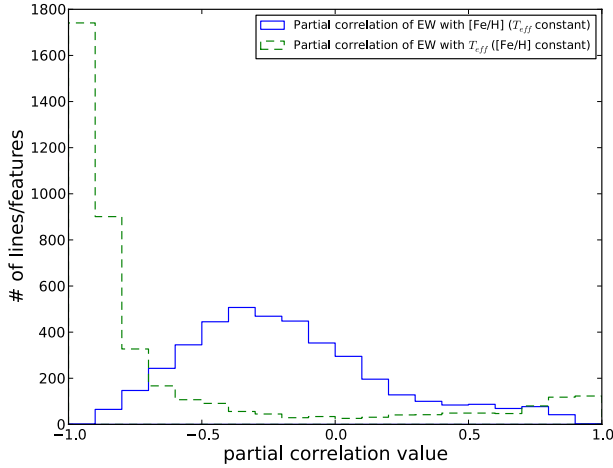


Fig. 2. Histograms of the partial correlations of [Fe/H] (solid blue histogram) and T_{eff} (dashed green histogram).

obtained 4104 lines/features. An automatic search of the maximum values around $\pm 0.02 \text{ \AA}$ at the extremes of each line/feature is made to make sure that the “peak-to-peak” regions of all lines/features of the spectra are effectively covered.

The next step consisted in the investigation of the correlation between the measured EWs and the reference values for [Fe/H] and T_{eff} . Figure 2 shows the histograms of the partial correlation coefficient values of the EWs with the value of the metallicity and effective temperature (solid blue and dashed green lines respectively). The partial correlation coefficient is defined as the correlation coefficient of one parameter keeping the other fixed. We observe, in Fig. 2 that a significant amount of lines have good correlation values with the parameters.

Then we did a least squares linear fit of the EWs with the metallicity and effective temperature. The reference values were calculated with the calibration of Neves et al. (2012), for [Fe/H], and with the three ($V - J$, $V - H$, and $V - K_S$) photometric calibrations of Casagrande et al. (2008), for T_{eff} , where we took the average value. From each line/feature i of every star m we calculate a EW value. Then we have

$$W_{i,m} = \alpha_i [\text{Fe}/\text{H}]_m^T + \beta_i T_{\text{eff},m}^T + \gamma_i, \quad (2)$$

where W is the matrix containing the EWs, and both $[\text{Fe}/\text{H}]^T$, and T_{eff}^T are the transpose vectors of the parameter values. The α and the β are the coefficients related to metallicity and effective temperature, respectively, while γ is an independent coefficient. The error associated to each parameter p is calculated as

$$\epsilon_p = \sqrt{RSS \cdot J_p}, \quad (3)$$

where RSS is the residual sum of squares, expressed as

$$RSS = \frac{\sum (x_{i,\text{model}} - x_i)^2}{n_{\text{obs}} - n_{\text{coef}}}, \quad (4)$$

and J is the diagonal of the estimate of the jacobian matrix around the solution. The $x_{i,\text{model}}$, x_i , n_{obs} , and n_{coef} from Eq. (3) are, respectively, the predicted value of the data, x_i , by the regression model, the data values, the number of data points, and the number of coefficients. We assume that both metallicity and effective temperature are independent and do not correlate with each other. This assumption was tested by perturbing each parameter in turn by introducing an positive or negative offset and then calculating both parameters. There was no difference in the

obtained values of the unperturbed parameter. We also tried to use the full covariance matrix to calculate the uncertainties but in the end we got a worse result for the dispersion. Therefore, we decided to use only the diagonal values of the covariance matrix. The total error of the coefficients associated to each line i can then be written as

$$\epsilon_i = \sqrt{\epsilon_\alpha^2 + \epsilon_\beta^2 + \epsilon_\gamma^2}. \quad (5)$$

The aim of our technique is to increase the precision of both [Fe/H] and T_{eff} determinations. To do that we need to obtain the values of the metallicity and effective temperature via a weighted least squares refit, that is obtained after a left multiplication of $(C^T C)^{-1} C^T$ on both terms of Eq. (2), where C is the calibration matrix or the coefficient matrix, that can be written as

$$C = \begin{bmatrix} \alpha_{1,1} & \beta_{1,2} & \gamma_{1,3} \\ \alpha_{2,1} & \beta_{2,2} & \gamma_{2,3} \\ \dots & \dots & \dots \\ \alpha_{I,1} & \beta_{I,2} & \gamma_{I,3} \end{bmatrix}, \quad (6)$$

and C^T is the transpose of C . The refit is then expressed, for each star m , as

$$\begin{bmatrix} [\text{Fe}/\text{H}] \\ T_{\text{eff}} \\ \Gamma \end{bmatrix} = (C^T C)^{-1} C^T W, \quad (7)$$

where Γ is the parameter related to the independent γ coefficients.

In order to correct the offset of our method we added an extra parameter, while adding a corresponding dimension in Eq. (6), that corresponds to an array of ones. The updated matrix C has now dimension $I \times 4$ instead of $I \times 3$, where I has the value of the number of lines.

Finally we introduce a weight to Eq. (7), using a *Levenberg-Marquardt* (Press et al. 1992) algorithm. We can write the elements of the normalised weight E as

$$E_i = \frac{1/\epsilon_i^2}{\sum 1/\epsilon_i^2}. \quad (8)$$

Other methods were tested, such as choosing lines/features with the best correlations or partial correlations with the parameters. However, the weighted least squares approach performed best at minimising the uncertainties of both metallicity and temperature.

2.2. A posteriori sample selection

At this stage we observed that some stars appeared as outliers in the plots of the pseudo EWs versus the reference [Fe/H] and T_{eff} for many lines. We suspected that this behaviour was due to activity or rotation and did a a posteriori study of the impact of the activity with our technique. To this end, we used the normalised $H\alpha$ luminosity, $\log L_{H\alpha}/L_{\text{bol}}$, from Reiners et al. (2012), for the stars in common with our full sample, as well as the median of individual measurements of the $H\alpha$ index defined by Gomes da Silva et al. (2011), kindly provided by the author. Table 4 lists both activity indicators, in Cols. 5 and 6, for the stars in common with our sample. Figure 3 depicts the relation between both indices, where we observe the inactive stars, in the bottom left corner of the diagram, a linear trend between the indices for increasingly active stars, and a very active star, Gl285, in the top right corner of diagram, where the $\log L_{H\alpha}/L_{\text{bol}}$ indicator seems to have saturated. The dashed black lines show the

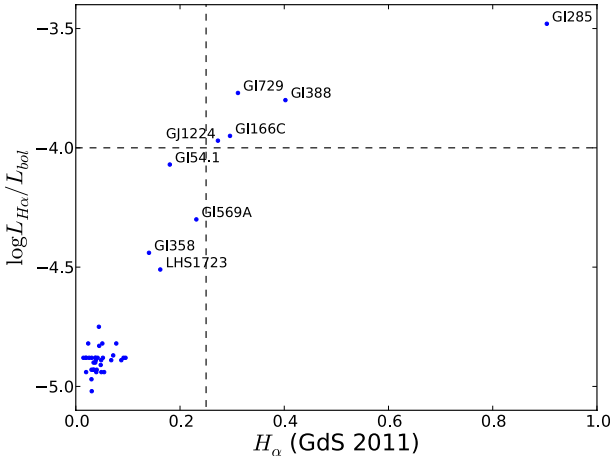


Fig. 3. Normalised $H\alpha$ luminosity, taken from [Reiners et al. \(2012\)](#) versus the $H\alpha$ index of [Gomes da Silva et al. \(2011\)](#) for the stars in common with our sample. The black dashed lines depict the limits that we have established for the sample selection.

limits above which the stars were excluded from the final sample, as described in the following paragraph.

Figure 4 displays the normalised $H\alpha$ luminosity and the $H\alpha$ index defined by [Gomes da Silva et al. \(2011\)](#) as a function of the difference between the parameters obtained with our method and the initial parameters. The legend in panels c) and d) depict the stellar spectra with $S/N \geq 100$ (blue dots), S/N between 30 and 100 (black crosses), S/N between 30 and 25 (red circles), and S/N lower than 25 (green stars). We observe no clear correlation of the activity indices or S/N with $[\text{Fe}/\text{H}]$. Regarding T_{eff} however, we can see that there is a clear trend towards lower temperatures with both activity indices. To take this trend into account we decided to perform an activity cut, excluding all stars with $\log L_{H\alpha}/L_{\text{bol}} \geq -4.0$ and $H\alpha \geq 0.25$ from our final sample. We also note a trend of $H\alpha$ with T_{eff} towards higher temperatures for stars with $S/N < 25$ (see bottom right corner of Fig. 4 d). The trends of our method with S/N are studied in detail in Sect. 2.4.

In the end, with a final sample of 65 stars, we obtain a dispersion of 0.08 dex for the metallicity and 91 K for the effective temperature, as shown in Fig. 5. The technique is valid between -0.85 to 0.26 dex for $[\text{Fe}/\text{H}]$, 2800 to 4100 K for T_{eff} , and between M0.0 to M5.0. The dispersion around the calibration is quantified by the root mean square error (RMSE), and defined as

$$\text{RMSE} = \sqrt{\frac{\sum (x_i - x_{\text{ref}})^2}{n_{\text{obs}} - n_{\text{coef}}}}, \quad (9)$$

where x_i is the estimated quantity, x_{ref} the reference value for the same quantity, n_{obs} the number of calibrators and n_{coef} the number of parameters used in the method (four in this case).

The calculated parameters as well as the reference determinations for $[\text{Fe}/\text{H}]$ and T_{eff} are listed in Table 2. Columns 1 and 3 contain the values for the reference calibrations, while Cols. 2 and 4 show the values obtained with our technique. We emphasise here that we only get an improvement on the precision. The accuracy of the method as well as its systematics are tied to the original determinations of the parameters.

2.3. Estimation of the uncertainties

To validate our method and have a better understanding of the uncertainties of our measurements we performed a bootstrap resampling and calculated the root mean square error of validation (RMSE_V).

Table 3. Uncertainty estimators for $[\text{Fe}/\text{H}]$ and T_{eff} .

Estimator	$[\text{Fe}/\text{H}]$ [dex]	T_{eff} [K]
RMSE	0.08	91
Bootstrap	0.08 ± 0.01	91 ± 13
RMSE_V	0.12	293

The bootstrap method we implemented tests how the rms of the method changes when using slightly different “bootstrapped” samples. To have a statistical significant number we first created 10 000 virtual samples by randomly drawing with repetition, for each virtual sample, a number of stars equal to the size of our sample. The random drawing followed a random uniform distribution. Then we calculated the rms for each trial and measured the 1σ gaussian equivalent interval between 15.9% and 84.1% from the resulting distribution, following the procedure of e.g. [Burgasser et al. \(2003\)](#); [Neves et al. \(2013\)](#). The distributions of the rms for both parameters are depicted in Fig. 6. The final result shows a variation of the rms of the $[\text{Fe}/\text{H}]$ and T_{eff} by ± 0.01 dex and ± 13 K respectively.

The calculation of the RMSE_V is a predicted residual sum of squares (PRESS) procedure ([Weisberg 2005](#)) and follows the description in the Appendix of [Rojas-Ayala et al. \(2012\)](#). In short, we try to obtain the original value of the metallicity and temperature of each star i of the technique leaving that star out when calculating the parameters. Then, we calculate the residuals, or the difference between the original and obtained value for each star and add them up in quadrature. The PRESS statistic is then defined as

$$\text{PRESS} = \sum (y_i - y_{\text{ref}})^2, \quad (10)$$

where y_i is the estimated value of the parameter and y_{ref} is the reference value of the measured quantity. From here we can calculate the root mean squared error of validation,

$$\text{RMSE}_V = \sqrt{\frac{\text{PRESS}}{n_V}}, \quad (11)$$

where n_V is the number of calibrators. The RMSE_V value can then be used to obtain confidence intervals. We obtain a RMSE_V value of 0.12 dex and ~ 293 K for the $[\text{Fe}/\text{H}]$ and T_{eff} respectively and will use these values as 1σ confidence intervals, assuming a normal cumulative distribution function. Table 3 summarises our results.

We observe that the uncertainties calculated with the different techniques are consistent with each other. The uncertainty for T_{eff} is large but is in line with the expected uncertainties. We also perturbed our sample by introducing an offset in $[\text{Fe}/\text{H}]$ or T_{eff} , as explained in Sect. 2.1 but found that it does not affect the measurement of the parameters. In the end we assume our final uncertainty to be the maximum uncertainty of the RMSE given by the bootstrap, that translates into 0.09 dex for $[\text{Fe}/\text{H}]$ and 110 K for T_{eff} .

2.4. Testing our technique as a function of resolution and S/N

To further test our method, we calculated the dispersion of the parameters as a function of the resolution and S/N . The first step consisted in the study of the behaviour of the procedure as a function of S/N only. We injected random Gaussian noise in the spectra of the sample to obtain spectra with $S/N @ 5500 \text{ \AA}$ between 100 and 10. Then, we calculated linear fits between

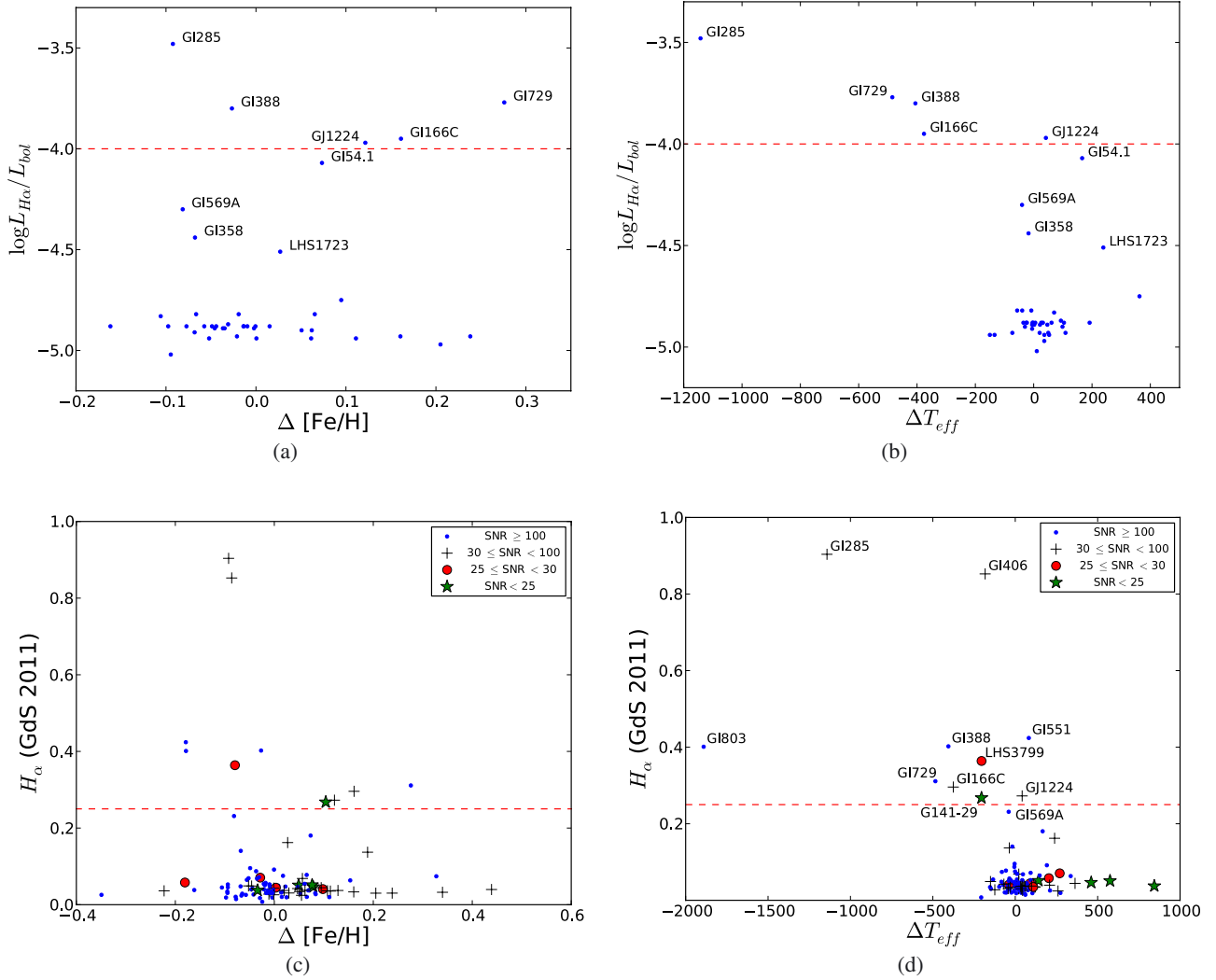


Fig. 4. **a)** Normalised $H\alpha$ luminosity taken from [Reiners et al. \(2012\)](#) as a function of $\Delta[\text{Fe}/\text{H}]$; **b)** normalised $H\alpha$ luminosity taken from [Reiners et al. \(2012\)](#) as a function of ΔT_{eff} ; **c)** $H\alpha$ index defined by [Gomes da Silva et al. \(2011\)](#) versus $\Delta[\text{Fe}/\text{H}]$; **d)** $H\alpha$ index defined by [Gomes da Silva et al. \(2011\)](#) versus ΔT_{eff} . The stars in common were taken from our full sample. The red dashed lines mark the limits above which the stars were excluded from the final sample.

the $[\text{Fe}/\text{H}]$ and T_{eff} obtained with the lower S/N spectra and the values of our method, for the full S/N range, as shown in Fig. 7 for $[\text{Fe}/\text{H}]$ and $S/N = 50$. The dashed black line marks the identity line while the red line represents a linear fit to the data.

Figure 8 depicts the slope and offset of the linear fits for $[\text{Fe}/\text{H}]$ and T_{eff} , as a function of S/N. We observe a deviation from the identity line as the S/N decreases as expected, except in d), where the offset of T_{eff} is reasonably constant, on average, with S/N. From here we investigated the cause of this trend and found that the measured EWs, roughly quantified as the median of all EWs, follow similar trends with S/N, as shown in Fig. 9 for the star GJ479 ($[\text{Fe}/\text{H}] = 0.01$ dex, $T_{\text{eff}} = 3218$ K) as example. The observed trends are similar in other stars, with different metallicities and effective temperatures.

Using this information, we corrected the values of both parameters for all stars of our sample with $S/N < 100$, where $[\text{Fe}/\text{H}]$ (Corrected) = $a[\text{Fe}/\text{H}]$ (Degraded) + b , and T_{eff} (Corrected) = aT_{eff} (Degraded) + b . The a is the slope and b is the offset. The uncertainties associated with each correction were estimated by calculating the dispersion of the residuals. However, we observed that these uncertainties are very small

compared to the final uncertainty of our method, as shown in Sect. 2.3. Therefore, we assumed the uncertainty of our method for all stars, except for the active ones, according to the two estimated activity thresholds calculated in Sect. 2.2. In this case, we used the initial values of the parameters, calculated with the calibrations of [Neves et al. \(2012\)](#) and [Casagrande et al. \(2008\)](#). At this point, we also decided not to use our new values for stars with $S/N \leq 25$, because the correction was not good enough to obtain a reasonable value for the objects depicted as green stars in Fig. 4. Moreover, we note that the stars LHS 1513 and GJ 803 give an estimated $[\text{Fe}/\text{H}]$ value of -1.51 and 0.46 dex respectively, calculated with the calibration of [Neves et al. \(2012\)](#), our reference scale. Both values are outside the range of this method and will not be used. Table 4 shows the corrected results, along with the previous values of $[\text{Fe}/\text{H}]$ from [Neves et al. \(2013\)](#). Column 1 describes the star designation and Cols. 2 and 3, the right ascension and declination of the star, respectively. Column 4 depicts the S/N, Col. 5 the normalised $H\alpha$ index taken from [Reiners et al. \(2012\)](#), and Col. 6 the $H\alpha$ index described by [Gomes da Silva et al. \(2011\)](#). Column 7 shows the metallicity calculated with the coefficient matrix used in our

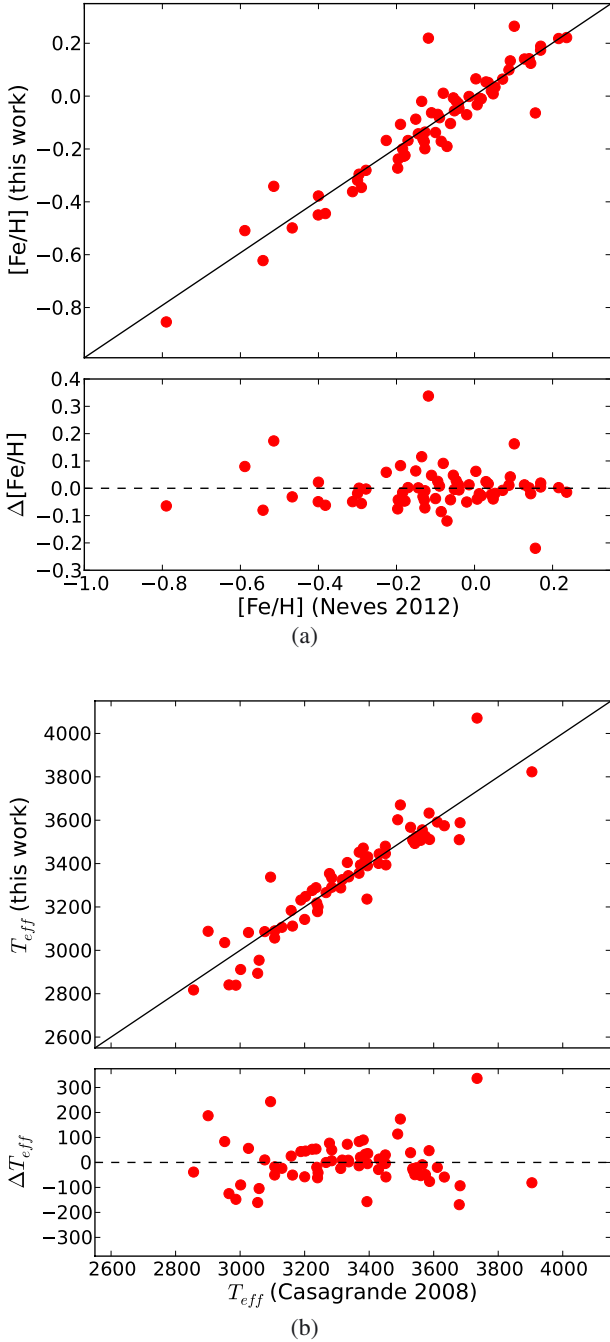


Fig. 5. **a)** $[\text{Fe}/\text{H}]$ comparison between this work and the photometric calibration of [Neves et al. \(2012\)](#); **b)** T_{eff} comparison between this work and the photometric calibration of [Casagrande et al. \(2008\)](#).

previous work, [Neves et al. \(2013\)](#), Col. 8 the $[\text{Fe}/\text{H}]$ obtained in our work, along with its associated error in Col. 9. The T_{eff} values of our stars, and its uncertainties are described in Cols. 10 and 11.

In the second step of this test we modified both resolution and S/N of our sample spectra. The resolution of the HARPS spectra was degraded by convolving the spectra with a normalised Gaussian curve, simulating the instrumental profile, with $FWHM = \lambda/R$, where λ is the wavelength and R the resolution we intend to obtain. From here, the standard deviation of the Gaussian is calculated with the well known formula

$$\sigma = \frac{FWHM}{2\sqrt{2\log 2}}. \quad (12)$$

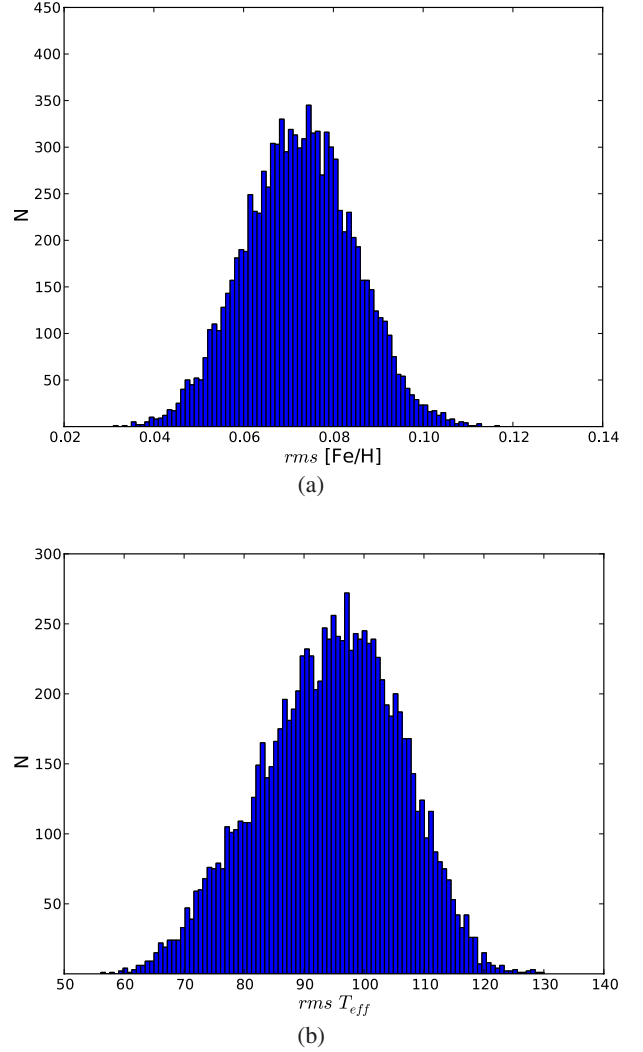


Fig. 6. Dispersion given by bootstrap for $[\text{Fe}/\text{H}]$ **a)** and T_{eff} **b)**. The N is the number of trials.

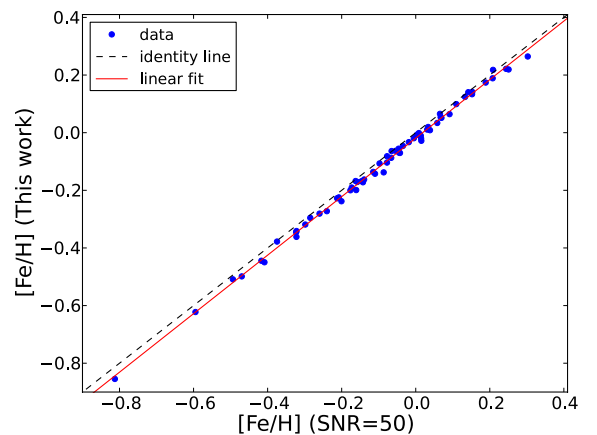


Fig. 7. $[\text{Fe}/\text{H}]$ of our procedure versus the $[\text{Fe}/\text{H}]$ obtained with $S/N = 50$. The identity line is depicted in dashed black. The solid red line shows the linear fit.

The σ was adjusted to the HARPS resolution ($R \sim 115.000$) and to the original S/N @ 5500 \AA of each spectrum. The final value for σ is then

$$\sigma' = \sqrt{\sigma^2 - \sigma_{\text{HARPS}}^2}. \quad (13)$$

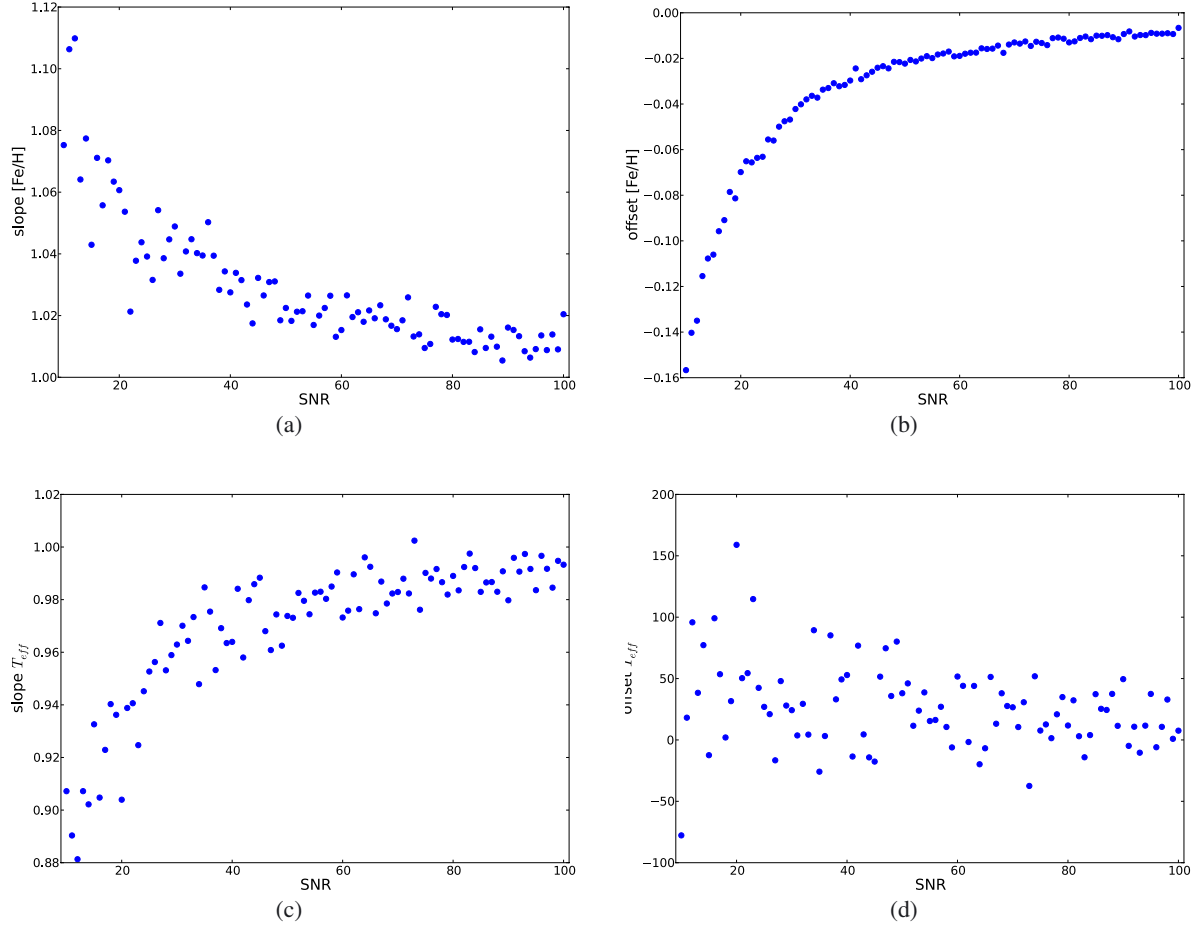


Fig. 8. Slope and offset of [Fe/H] and T_{eff} of our work as a function of S/N for star G1479.

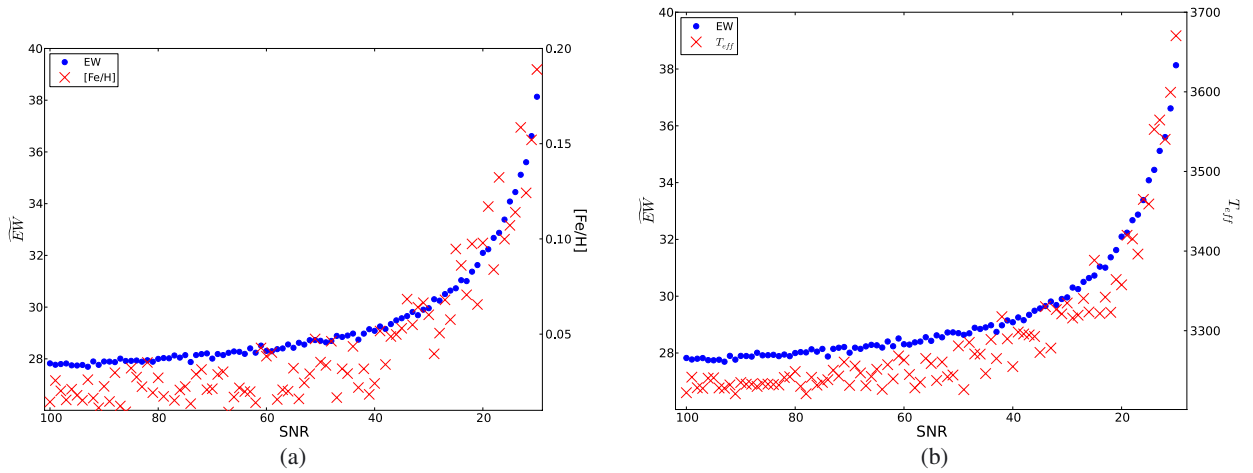


Fig. 9. Median of the pseudo EWs and [Fe/H] **a)** or T_{eff} **b)** as a function of S/N for star G1479.

Figures 10 and 11 show the difference of our parameters against the degraded values, as a function of resolution (while the S/N is kept constant at 100) and as a function of S/N (while the resolution is kept constant at 100.000) for [Fe/H] and T_{eff} respectively. The red dotted line depicts the offset of the residuals.

From the two figures we observe the existence of linear trends for different resolutions and S/N. To correct these trends we performed a linear fit for each Resolution/signal-to-noise

combination with the functional form [Fe/H] (This work) = $a[\text{Fe/H}]$ (Degraded) + b for metallicity, and T_{eff} (This work) = aT_{eff} (Degraded) + b for effective temperature. The values for each combination are shown in Table 5.

From here we calculated the dispersion of the difference between the corrected parameter values and the ones obtained from our original determinations, and added this dispersion with the one from our method in quadrature. Table 6 shows the results.

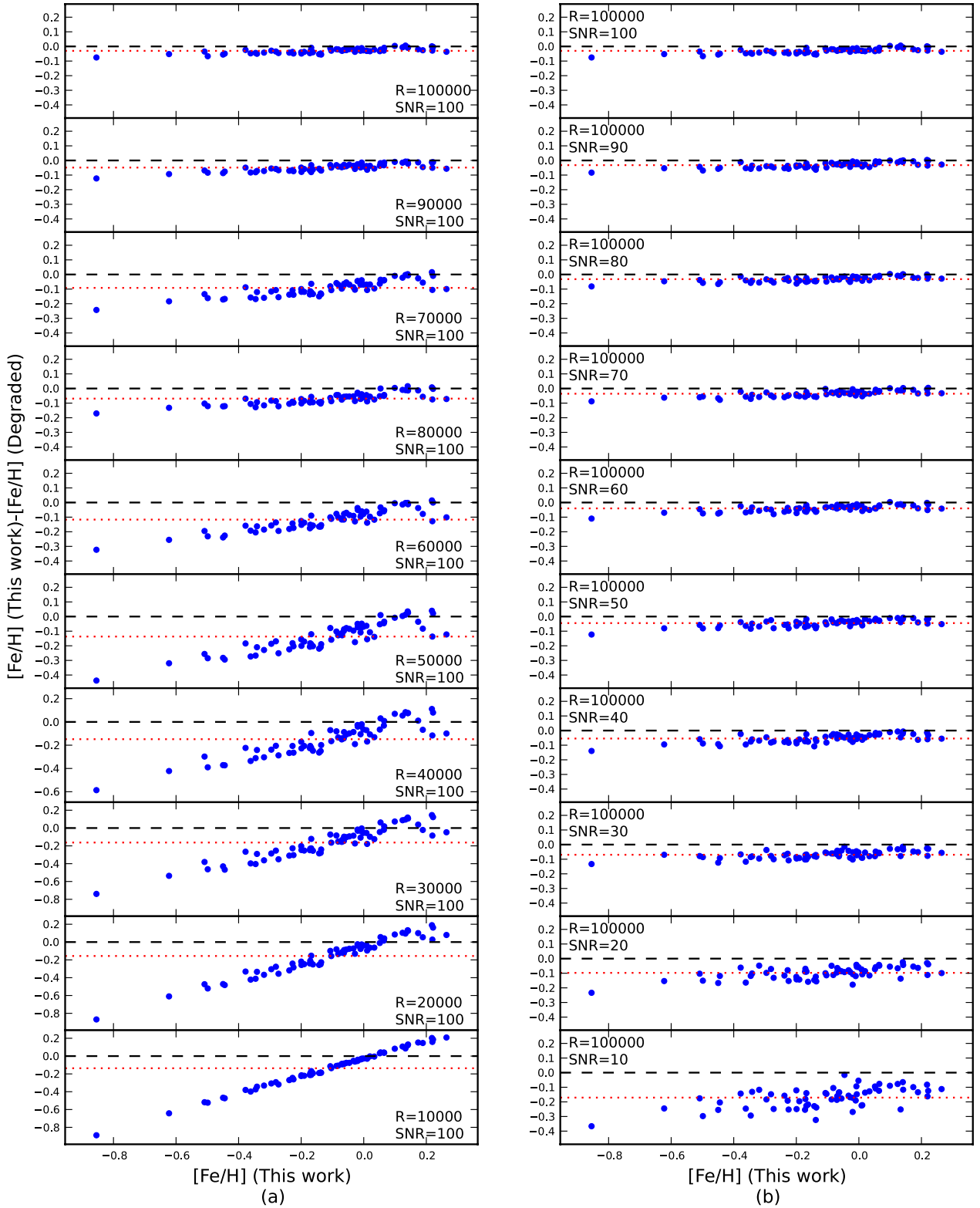


Fig. 10. Difference of the $[\text{Fe}/\text{H}]$ for this work and the $[\text{Fe}/\text{H}]$ calculated with different resolution/signal-to-noise combinations as a function of the resolution and S/N.

The horizontal header of both tables correspond to the S/N of the spectra, between 100 and 10, while the vertical header depicts their resolution, from 100 000 to 10 000. The row with the resolution number is the value of the dispersion of our technique using the corresponding resolution/signal-to-noise combination. This table should be used as a guideline for the uncertainties of the parameters when using spectra other than HARPS.

From Table 6 and Figs. 10 and 11 we observe that, as the resolution degrades, the dispersion and offset of the residuals increase. In the case of $[\text{Fe}/\text{H}]$, the dispersion value holds well for a resolution higher and equal to 40 000 respectively. From 35 000 and lower resolutions we observe that the uncertainties of the residuals are similar or greater than the original dispersion (0.17 dex), meaning that the method is not useful any

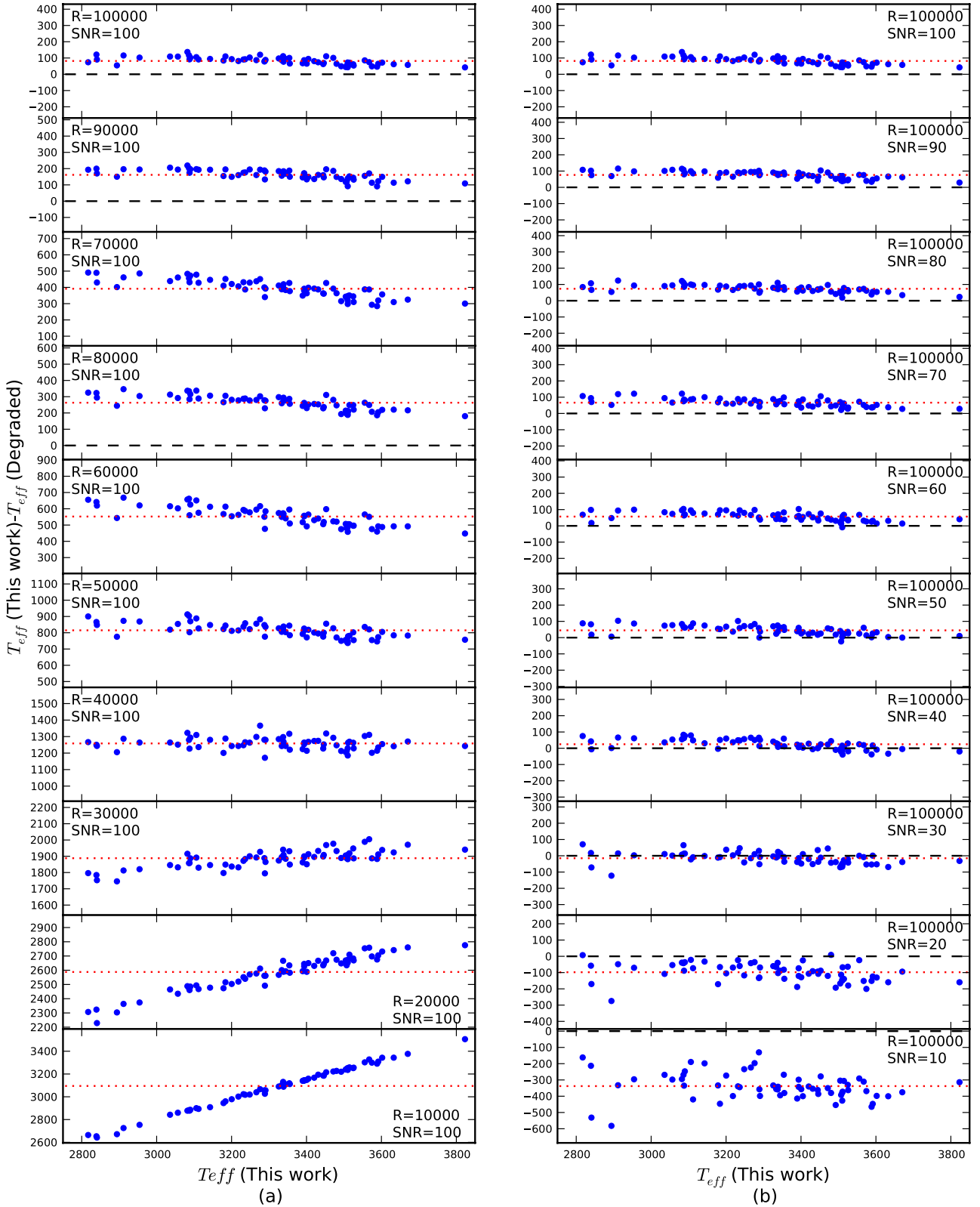


Fig. 11. Difference of the T_{eff} for this work and the T_{eff} calculated with different resolution/signal-to-noise combinations as a function of the resolution and S/N.

more, providing we have precise parallaxes and visual magnitudes. Regarding T_{eff} , we consider that the method is valid for the same resolution and S/N intervals as in [Fe/H]. We also limit the use of the technique for spectra with S/N greater than 25, as we cannot properly correct the parameters, as we have previously seen in this section. From here we investigated the nature

of these correlations by plotting the median of all EWs with the parameters, as a function of resolution (with $S/N = 100$), for a metal-poor star G1191 ([Fe/H] = -0.85 dex, $T_{\text{eff}} = 3510$ K) and a metal-rich star, GJ 317 ([Fe/H] = 0.22 dex, $T_{\text{eff}} = 3106$ K), as it was previously done for S/N, and shown in Fig. 9. Figure 12 pictures the results. The blue dots depict the median of the

Table 5. Linear fit coefficients a and b from the relation between the values of our parameters and the values calculated for different combinations of resolution and S/N.

		(a) [Fe/H]									
S/N	Resolution	100		90		80		70		60	
		a	b	a	b	a	b	a	b	a	b
100 000		1.0573	-0.0257	1.0645	-0.0269	1.0572	-0.0275	1.0721	-0.0304	1.0686	-0.0353
95 000		1.0793	-0.0304	1.0786	-0.0343	1.0849	-0.0358	1.0766	-0.0401	1.0740	-0.0455
90 000		1.0947	-0.0428	1.1111	-0.0430	1.0973	-0.0472	1.1024	-0.0488	1.1029	-0.0521
85 000		1.1164	-0.0529	1.1345	-0.0511	1.1313	-0.0557	1.1451	-0.0592	1.1209	-0.0639
80 000		1.1522	-0.0630	1.1527	-0.0652	1.1545	-0.0670	1.1595	-0.0694	1.1587	-0.0749
75 000		1.1819	-0.0751	1.1859	-0.0790	1.1774	-0.0801	1.1891	-0.0838	1.1967	-0.0877
70 000		1.2184	-0.0877	1.2271	-0.0905	1.2309	-0.0920	1.2354	-0.0939	1.2441	-0.1018
65 000		1.2614	-0.0997	1.2781	-0.1045	1.2739	-0.1075	1.2850	-0.1094	1.2849	-0.1149
60 000		1.3350	-0.1191	1.3306	-0.1174	1.3361	-0.1206	1.3408	-0.1255	1.3437	-0.1305
55 000		1.3949	-0.1372	1.4058	-0.1370	1.4039	-0.1417	1.3962	-0.1439	1.4440	-0.1518
50 000		1.4859	-0.1499	1.5020	-0.1559	1.5317	-0.1590	1.5211	-0.1631	1.5289	-0.1666
45 000		1.5768	-0.1623	1.5924	-0.1670	1.5550	-0.1700	1.5998	-0.1726	1.5686	-0.1811
40 000		1.6667	-0.1739	1.6608	-0.1837	1.6628	-0.1912	1.6434	-0.1903	1.6910	-0.1976
35 000		1.6830	-0.1907	1.7071	-0.1930	1.7183	-0.1984	1.6553	-0.2061	1.6662	-0.2076
30 000		1.7031	-0.1998	1.6868	-0.2016	1.6715	-0.2080	1.6561	-0.2102	1.6526	-0.2109
25 000		1.7480	-0.2035	1.7205	-0.2016	1.7607	-0.2103	1.7139	-0.2077	1.7232	-0.2126
20 000		1.8697	-0.1965	1.8721	-0.1996	1.9415	-0.2054	1.7788	-0.1984	1.7328	-0.1986
15 000		2.2339	-0.1950	2.1304	-0.1933	2.3825	-0.2044	2.4904	-0.2125	2.3611	-0.2164
10 000		3.6228	-0.2062	2.6636	-0.1899	2.8711	-0.1999	2.6645	-0.2022	0.1404	-0.1154
S/N	Resolution	50		40		30		20		10	
		a	b	a	b	a	b	a	b	a	b
100 000		1.0749	-0.0400	1.0863	-0.0496	1.0652	-0.0669	1.0962	-0.0962	1.1196	-0.1781
95 000		1.1026	-0.0480	1.0960	-0.0566	1.0912	-0.0775	1.1092	-0.1012	1.0946	-0.1912
90 000		1.1050	-0.0574	1.1229	-0.0683	1.1226	-0.0842	1.1506	-0.1184	1.1492	-0.2043
85 000		1.1322	-0.0698	1.1658	-0.0794	1.1645	-0.0921	1.1767	-0.1251	1.1727	-0.2200
80 000		1.1730	-0.0826	1.1852	-0.0877	1.2021	-0.1082	1.2164	-0.1443	1.1864	-0.2345
75 000		1.2013	-0.0947	1.2168	-0.1039	1.2283	-0.1229	1.2608	-0.1553	1.1913	-0.2321
70 000		1.2298	-0.1103	1.2395	-0.1177	1.2697	-0.1359	1.2593	-0.1605	1.2609	-0.2620
65 000		1.3065	-0.1210	1.3072	-0.1315	1.3125	-0.1482	1.3743	-0.1880	1.2488	-0.2867
60 000		1.3658	-0.1417	1.3886	-0.1524	1.3698	-0.1694	1.3925	-0.1991	1.2093	-0.2847
55 000		1.4498	-0.1584	1.4282	-0.1685	1.4266	-0.1878	1.4316	-0.2206	1.4105	-0.3137
50 000		1.5178	-0.1755	1.5140	-0.1952	1.5464	-0.2043	1.5296	-0.2523	1.2569	-0.3076
45 000		1.6032	-0.1942	1.5460	-0.2028	1.6107	-0.2200	1.5216	-0.2526	1.2952	-0.3159
40 000		1.6677	-0.2050	1.5879	-0.2159	1.5324	-0.2321	1.4905	-0.2579	1.2183	-0.3194
35 000		1.6524	-0.2123	1.6276	-0.2232	1.6483	-0.2486	1.4189	-0.2579	1.0835	-0.2904
30 000		1.7535	-0.2277	1.6359	-0.2315	1.5524	-0.2371	1.4348	-0.2617	1.0072	-0.2814
25 000		1.7370	-0.2223	1.5786	-0.2180	1.6060	-0.2398	1.5160	-0.2570	0.9624	-0.2582
20 000		1.7250	-0.2059	1.8548	-0.2279	1.6821	-0.2321	1.1003	-0.2154	0.8352	-0.2465
15 000		1.6573	-0.1903	1.7403	-0.2065	1.9868	-0.2428	1.0153	-0.2100	0.3012	-0.1615
10 000		1.5151	-0.1772	1.3777	-0.1797	0.8703	-0.1678	1.2768	-0.2351	0.5612	-0.2087

pseudo EWs while the red crosses show the metallicity or the effective temperature.

We observe that the EW and the parameters follow similar trends as the resolution degrades, as expected (except in Fig. 12a) where metallicity has an opposite trend to the EW. We do not know the cause of the different trend.

The increasing dispersions and offsets with the resolution observed in Figs. 10 and 11 should originate from the nature of our “peak-to-peak” technique because it does not consider the continuum. As the resolution gets worse, more and more flux from the “peak-to-peak” region is lost to the line wings. However, as the resolution decreases there is an increase of line blending that makes the measurement of the correct flux of the each line/feature increasingly difficult. Moreover, we also observe from Fig. 2 that we have similar numbers of correlation and anti-correlations of the lines with [Fe/H], and the overall effect of the weighted lines may change as the resolution degrades. The mix of any of these effects may be the reason behind we get different trends for [Fe/H] from G1191 (Fig. 12a) and GJ436 (Fig. 12c).

In order to validate our estimation of the uncertainties we used a sample of spectra of stars in common taken from the SOPHIE spectrograph (Bouchy & The Sophie Team 2006) archive². We downloaded individual observations taken with the “HR” ($R \sim 75\,000$) and “HE” ($R \sim 40\,000$) modes, with the reference fiber exposed to the sky rather than to the thorium–argon calibration lamp, to avoid potential contamination. The “HR” sample is comprised of 12 stars in common while the “HE” sample contains only 5 stars.

First, we summed the individual spectra of each star, after correcting the radial velocity of each spectrum, and calculated their pseudo EWs. The S/N of the summed spectra for each star in common range from 34 to more than 600. Then, we calculated the metallicity and effective temperature and applied the appropriate corrections shown in Table 5, following the resolution and S/N of each spectra. The final values of the parameters are displayed in Table 7. Column 2 lists the resolution, Col. 3

² <http://atlas.obs-hp.fr/sophie/>

Table 5. continued.

(b) T_{eff}										
S/N Resolution	100		90		80		70		60	
	a	b								
100 000	0.9391	279	0.9395	273	0.9394	271	0.9306	293	0.9294	288
95 000	0.9305	342	0.9156	387	0.9182	377	0.9098	396	0.9164	364
90 000	0.9137	435	0.8986	482	0.9167	416	0.9087	435	0.9028	447
85 000	0.8802	582	0.8873	558	0.8811	575	0.8729	590	0.8879	538
80 000	0.8726	654	0.8705	658	0.8646	672	0.8676	655	0.8524	694
75 000	0.8524	767	0.8502	769	0.8497	767	0.8444	778	0.8511	750
70 000	0.8339	880	0.8360	872	0.8478	829	0.8305	876	0.8418	830
65 000	0.8286	957	0.8290	952	0.8277	953	0.8396	912	0.8354	917
60 000	0.8298	1025	0.8240	1039	0.8457	977	0.8389	989	0.8576	932
55 000	0.8553	1050	0.8583	1040	0.8743	994	0.8712	997	0.8711	993
50 000	0.8864	1101	0.8870	1096	0.8892	1088	0.8896	1083	0.9061	1036
45 000	0.9083	1227	0.9243	1184	0.9139	1204	0.9318	1159	0.9243	1169
40 000	0.9733	1313	0.9820	1294	0.9832	1284	0.9873	1274	1.0037	1227
35 000	1.0585	1451	1.0587	1445	1.0673	1424	1.0664	1414	1.0656	1408
30 000	1.2080	1587	1.2091	1573	1.2198	1554	1.2030	1565	1.2386	1498
25 000	1.4745	1717	1.4831	1699	1.4847	1683	1.5107	1641	1.5034	1624
20 000	1.9977	1842	2.0116	1817	1.9598	1834	1.9840	1793	1.9362	1792
15 000	3.1029	1946	3.1103	1914	2.9692	1936	3.0119	1867	3.0566	1775
10 000	6.8985	1681	6.2175	1775	6.2539	1685	6.2833	1548	5.6847	1562
S/N Resolution	50		40		30		20		10	
	a	b								
100 000	0.9249	291	0.9223	281	0.9363	198	0.9001	245	0.8592	179
95 000	0.9148	358	0.9194	327	0.9000	352	0.8961	290	0.8793	130
90 000	0.9083	419	0.8891	459	0.8993	390	0.8898	353	0.8804	161
85 000	0.8733	572	0.8741	547	0.8894	462	0.8595	492	0.8308	361
80 000	0.8665	640	0.8566	647	0.8626	597	0.8649	512	0.8964	178
75 000	0.8492	742	0.8506	714	0.8534	674	0.8623	571	0.8284	465
70 000	0.8494	796	0.8407	806	0.8479	750	0.8816	572	0.8621	402
65 000	0.8438	878	0.8257	915	0.8466	816	0.8567	713	0.8433	519
60 000	0.8477	948	0.8705	863	0.8817	797	0.8801	725	0.9280	332
55 000	0.8968	912	0.8730	954	0.8778	913	0.8882	817	0.8757	608
50 000	0.9027	1032	0.9235	962	0.9400	889	0.9670	730	0.9068	629
45 000	0.9462	1109	0.9496	1078	0.9855	956	1.0141	791	1.0176	467
40 000	1.0046	1211	1.0191	1157	1.0381	1074	1.0690	901	0.9749	794
35 000	1.1054	1317	1.1249	1252	1.1198	1204	1.1365	1059	1.0122	939
30 000	1.2608	1441	1.2615	1401	1.2422	1353	1.2352	1216	1.2106	780
25 000	1.5634	1525	1.5462	1491	1.4461	1513	1.4680	1287	1.1921	1163
20 000	2.0226	1665	2.0712	1542	1.9740	1475	1.8071	1364	1.3502	1271
15 000	3.0308	1698	2.8844	1623	2.7979	1454	2.3031	1400	1.4130	1486
10 000	4.8757	1643	4.4861	1557	3.1564	1817	1.9481	2046	0.3888	2893

the S/N , and Cols. 4 to 7 the parameters of our method and the ones obtained with the SOPHIE spectra, respectively.

We obtain a rms for the $[\text{Fe}/\text{H}]$ of 0.088 and 0.123 dex for the “HR” and the “HE” samples respectively. Both dispersions are very close the expected dispersions for $R = 75\,000$ and $R = 40\,000$, as depicted in Table 6. For T_{eff} , we obtain a dispersion of 104 and 172 K for the “HR” and “HE” samples respectively. Both values are above the expected values, but in the case of the “HR” sample, the difference is only a few Kelvin. Regarding the “HE” sample, this difference is larger (~ 75 K), but the dispersion value is close to the one considered for the photometric calibration (~ 150 K). Moreover, we note that the sample size is very small ($N = 5$). These results give us confidence and validate our uncertainty estimation method.

3. Comparison with the literature

A comparison with other studies in the literature was performed. This comparison allow us to evaluate the accuracy of our method

and the possible systematics that it may suffer. Table 8 shows our spectroscopic results compared to the ones found in the literature, for the stars in common. Column 1 depicts the star designations and Col. 2 informs if the star belongs or not to the selected sample that we used to calibrate our method. Columns 3 to 13 and Cols. 14 to 21 describe our $[\text{Fe}/\text{H}]$ and T_{eff} against the metallicity found in the literature, respectively. We note here that we only used the spectroscopic derived values for comparison. All active stars were excluded from this exercise.

We show in Table 9 the results of the comparison for the sample used in our technique and the full sample. The results for $[\text{Fe}/\text{H}]$ are separated by photometric and spectroscopic techniques. The first column depicts the name of the method along with its reference. Column two and three describe the dispersion and offset. The last column reports the number of stars in common with our sample. We do not display the calibration of Mann et al. (2013a) in Table 9 because we only have two stars in common with them. However, we include the 4 measurements from the V - and K -band calibrations in the row “All $[\text{Fe}/\text{H}]$ values”. We note here that we only compared stars in common for which

Table 6. Dispersion of the residuals of the parameters as a function of the resolution and S/N.

		(a) [Fe/H]									
S/N		100	90	80	70	60	50	40	30	20	10
Resolution											
100 000		0.081	0.081	0.081	0.081	0.082	0.082	0.083	0.083	0.089	0.105
95 000		0.082	0.082	0.082	0.082	0.082	0.083	0.083	0.086	0.091	0.107
90 000		0.082	0.082	0.082	0.082	0.083	0.083	0.084	0.087	0.089	0.103
85 000		0.083	0.083	0.083	0.083	0.085	0.085	0.085	0.085	0.094	0.116
80 000		0.084	0.084	0.084	0.085	0.085	0.085	0.087	0.089	0.095	0.113
75 000		0.085	0.085	0.086	0.086	0.086	0.087	0.089	0.092	0.097	0.123
70 000		0.088	0.087	0.088	0.088	0.088	0.091	0.091	0.094	0.100	0.122
65 000		0.090	0.090	0.091	0.092	0.094	0.095	0.096	0.100	0.107	0.125
60 000		0.092	0.096	0.093	0.095	0.097	0.099	0.098	0.102	0.109	0.144
55 000		0.098	0.099	0.101	0.102	0.102	0.101	0.109	0.113	0.126	0.144
50 000		0.108	0.109	0.109	0.113	0.115	0.118	0.120	0.124	0.132	0.161
45 000		0.125	0.126	0.129	0.128	0.135	0.131	0.138	0.138	0.148	0.174
40 000		0.146	0.147	0.148	0.151	0.149	0.152	0.156	0.161	0.174	0.185
35 000		0.168	0.169	0.170	0.172	0.174	0.175	0.174	0.176	0.187	0.203
30 000		0.189	0.189	0.190	0.191	0.192	0.189	0.194	0.199	0.202	0.212
25 000		0.205	0.207	0.205	0.208	0.207	0.207	0.211	0.212	0.209	0.219
20 000		0.220	0.217	0.218	0.220	0.219	0.221	0.219	0.219	0.228	0.225
15 000		0.227	0.228	0.226	0.224	0.226	0.231	0.229	0.227	0.231	0.235
10 000		0.231	0.233	0.233	0.233	0.236	0.234	0.234	0.235	0.231	0.233

		(b) T_{eff}									
S/N		100	90	80	70	60	50	40	30	20	10
Resolution											
100 000		92	92	92	92	93	93	94	96	103	118
95 000		92	92	92	93	93	93	95	97	103	116
90 000		93	93	94	93	94	95	95	98	99	116
85 000		93	94	93	94	94	94	95	95	102	115
80 000		94	94	94	95	94	95	96	99	102	117
75 000		93	94	94	95	94	96	96	97	101	120
70 000		94	95	95	95	95	96	97	99	103	116
65 000		95	95	94	95	95	96	97	97	102	117
60 000		95	95	96	96	95	97	97	100	102	115
55 000		95	95	96	95	95	97	98	101	107	127
50 000		95	95	96	96	96	98	99	103	104	123
45 000		97	96	97	97	97	96	99	101	108	129
40 000		98	98	97	99	99	99	100	106	113	128
35 000		99	100	100	99	99	100	103	106	114	148
30 000		101	101	103	102	103	101	106	111	123	147
25 000		104	104	108	105	106	108	113	115	129	161
20 000		112	110	111	118	115	116	116	125	143	179
15 000		116	120	126	125	130	129	146	154	179	216
10 000		135	133	155	146	167	177	185	214	235	259

we could calculate precise values of [Fe/H] and T_{eff} with our methodology.

The photometric [Fe/H] was calculated with the relations of Bonfils et al. (2005), Schlafman & Laughlin (2010) and Johnson et al. (2012), while the spectroscopic [Fe/H] was taken directly from the works of Woolf & Wallerstein (2005), Rojas-Ayala et al. (2012), Önehag et al. (2012), Terrien et al. (2012), Newton (2013), and Mann et al. (2013b), except in the case of Mann et al. (2013a), where the values of the visible (their Eq. (8)) and K -band (their Eq. (16)) calibrations were provided directly by the author. We note that we used the average of the H - and K -band spectroscopic relations of Terrien et al. (2012). Also, we restricted the calculation of the photometric calibrations to the stars from the sample selection, for which we have precise photometries and parallaxes, to insure the best possible results in the comparison exercise.

Figure 13 portrays two [Fe/H]-[Fe/H] plots, with data taken from the selected sample. The left plot (a) shows the comparison of our sample with the works based on photometric scales.

The blue dots, red crosses and black plus signs indicate the results of Bonfils et al. (2005), Schlafman & Laughlin (2010), and Johnson et al. (2012) respectively. The right plot (b) depicts the comparison of our selected sample with other spectroscopic methods. The purple triangles, red crosses, red circles, green plus signs, black stars, black diamonds, black plus signs, and blue dots correspond to the measurements of Woolf & Wallerstein (2005), Rojas-Ayala et al. (2012), Önehag et al. (2012), Terrien et al. (2012), Mann et al. (2013a,b), and Newton (2013) respectively. The (V) and (K) in Mann et al. (2013a) correspond to measurements performed with a V - and K -band calibration respectively. The solid black line in the upper panel of both plots defines an identity line. The lower panels show the residuals. The dashed black line marks the zero-point of the calibration.

For metallicity we observe a general agreement between our results and the ones from the literature. We note here that the calibration of Schlafman & Laughlin (2010) is very similar to our reference calibration, from Neves et al. (2012), and this is the

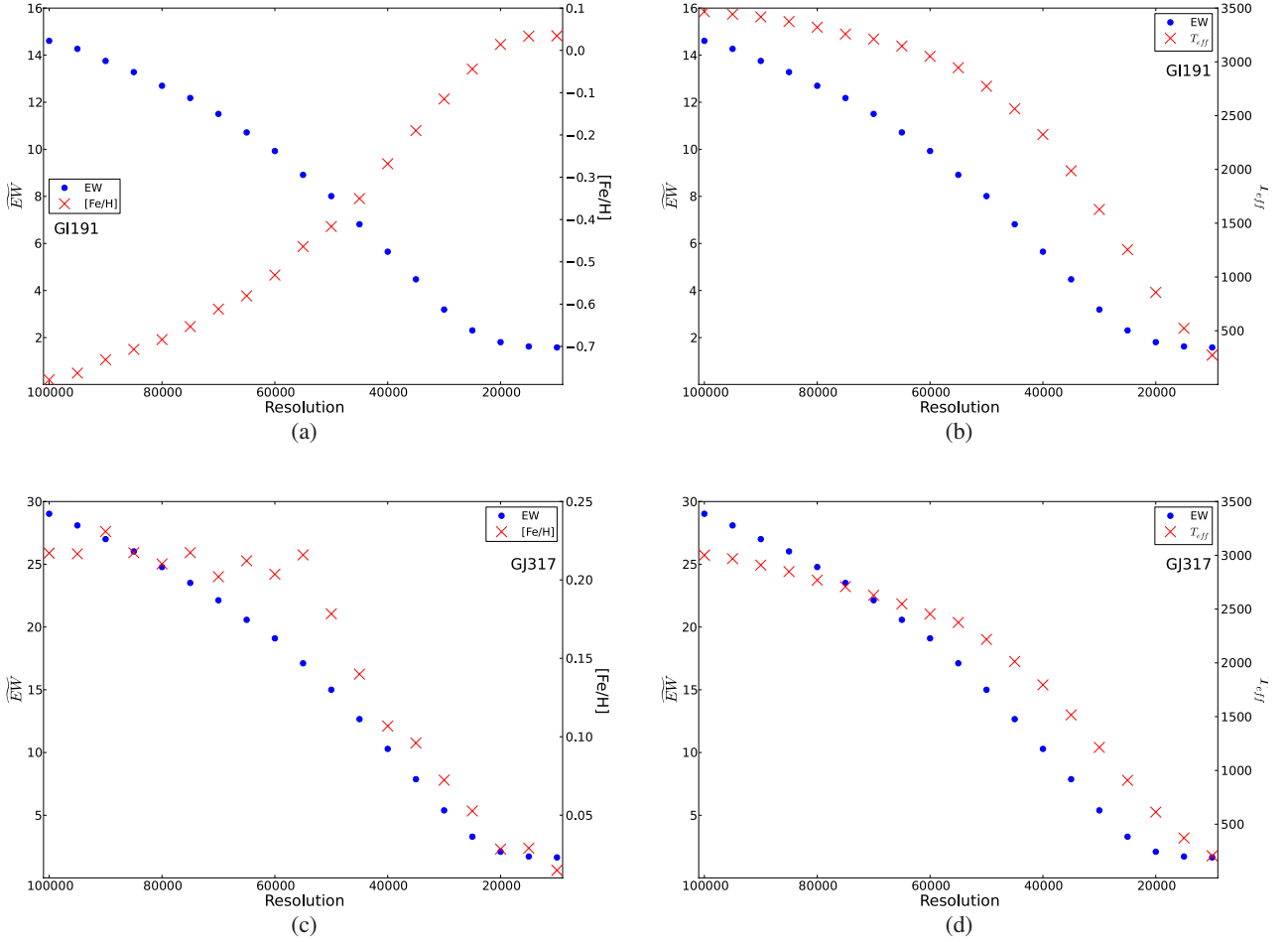


Fig. 12. Measured median of the pseudo EWs, $[\text{Fe}/\text{H}]$ and T_{eff} as a function of resolution for the stars G191 **a)** and **b)** and GJ317 **c)** and **d)**. The blue dots depict the median of the pseudo EWs while the red crosses show the metallicity or the effective temperature.

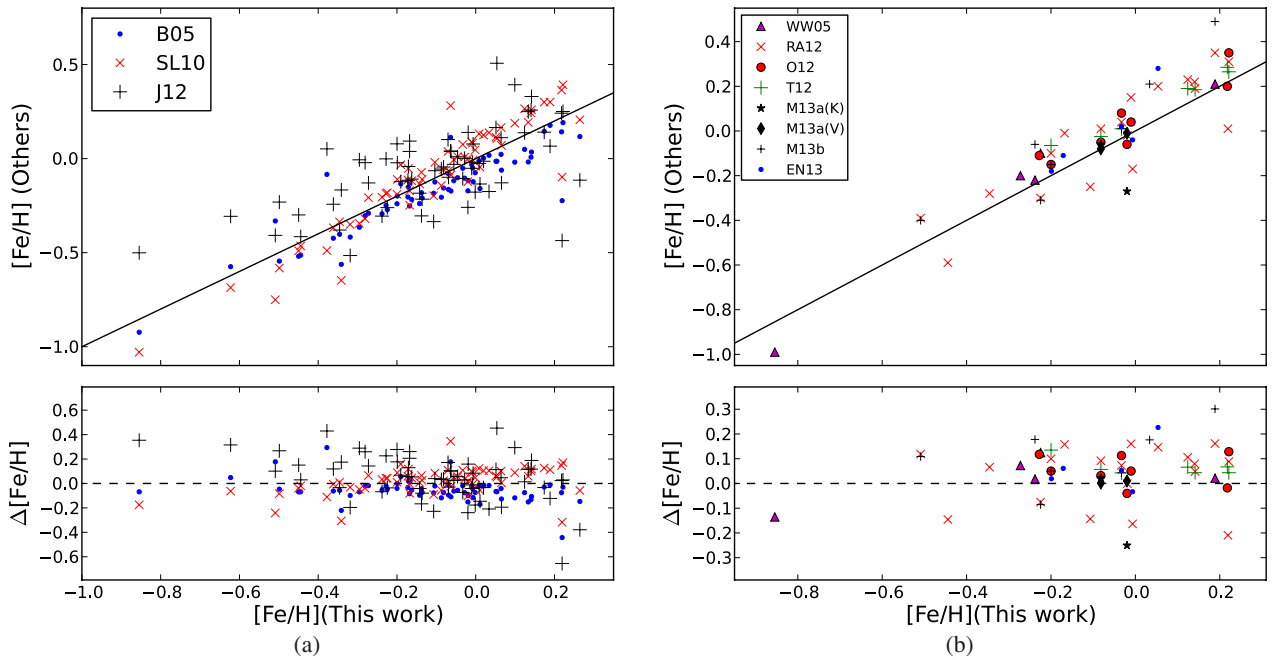


Fig. 13. Upper panel: $[\text{Fe}/\text{H}]-[\text{Fe}/\text{H}]$ plots comparing the values of this work, from the selected sample, against others in the literature. The solid black line of both **a)** and **b)** depict the identity line; lower panel: comparison plot residuals. The dashed black line marks the zero point of our technique. The plot **a)** shows the results of our work versus three photometric calibrations taken from the literature, while plot **b)** depicts the comparison between our results against other spectroscopic measurements.

Table 7. [Fe/H] and T_{eff} calculated from a sample in common with SOPHIE observations.

Star	Resolution	S/N	[Fe/H] (this work) [dex]	[Fe/H] (SOPHIE) [dex]	T_{eff} (this work) [K]	T_{eff} (SOPHIE) [K]
Gl699	75.000	102	-0.51	-0.39	3338	3292
Gl686	75.000	557	-0.35	-0.28	3493	3529
Gl87	75.000	147	-0.32	-0.21	3555	3472
GJ1125	75.000	64	-0.09	0.07	3112	3049
G1273	75.000	62	-0.01	-0.02	3090	3057
GJ2066	75.000	86	-0.17	-0.07	3421	3249
Gl393	75.000	91	-0.20	-0.10	3431	3326
Gl514	75.000	636	-0.16	-0.11	3526	3501
Gl846	75.000	175	0.01	0.04	3588	3551
Gl176	75.000	79	-0.01	0.06	3355	3196
GJ179	75.000	34	0.12	0.06	3086	2878
Gl436	75.000	150	-0.03	0.04	3354	3304
Gl447	40.000	56	-0.17	-0.15	3036	3202
Gl213	40.000	85	-0.11	-0.15	3082	3246
GJ1125	40.000	62	-0.09	-0.03	3112	3340
Gl846	40.000	79	0.01	0.27	3588	3762
GJ179	40.000	141	0.12	0.13	3086	3188

Table 9. Dispersion and offset of [Fe/H] and T_{eff} from the residuals of the sample of the method and full sample against other studies.

(a) Selected sample				
	rms	offset	N	
Photometric [Fe/H] calibrations				
Bonfils et al. (2005)	0.11	-0.06	65	
Schlaufman & Laughlin (2010)	0.11	0.02	65	
Johnson et al. (2012)	0.19	0.05	65	
Spectroscopic [Fe/H] determinations	rms	offset	N	
All [Fe/H] values	0.11	0.05	55	
Woolf & Wallerstein (2005)	0.09	-0.02	5	
Rojas-Ayala et al. (2012)	0.12	0.03	19	
Önehag et al. (2012)	0.08	0.05	8	
Terrien et al. (2012)	0.07	0.06	7	
Mann et al. (2013b)	0.16	0.11	7	
Newton (2013)	0.11	0.07	5	
T_{eff} determinations	rms	offset	N	
Woolf & Wallerstein (2005)	122	116	5	
Rojas-Ayala et al. (2012)	299	246	19	
Önehag et al. (2012)	160	64	8	
Boyajian et al. (2012)	157	129	49	
Mann et al. (2013b)	167	133	7	
Rajpurohit et al. (2013a)	132	100	8	
(b) Full Sample				
Spectroscopic [Fe/H] determinations	rms	offset	N	
Rojas-Ayala et al. (2012)	0.13	0.06	25	
Newton (2013)	0.15	0.1	13	
T_{eff} values	rms	offset	N	
Rojas-Ayala et al. (2012)	304	222	25	
Boyajian et al. (2012)	149	111	55	
Rajpurohit et al. (2013a)	181	133	12	

Notes. The last column shows the number of stars in common.

reason why we obtain a value of dispersion smaller than the one of the original calibration (0.11 vs. 0.17 dex). The dispersion of the oldest photometric calibration (Bonfils et al. 2005) is surprisingly low (0.11 dex), considering that the original dispersion for this calibration is 0.20 dex. However, the Bonfils et al. (2005) is also similar to Schlaufman & Laughlin (2010) and Neves et al. (2012) which may explain part of the low dispersion. Regarding the Johnson et al. (2012) calibration, we obtain a rms of 0.19 dex,

higher than their reported value of 0.15 dex. The dispersion of the spectroscopic determinations are within the expected values (~ 0.11 dex), considering the uncertainties of each method, except in the case of Mann et al. (2013b), where we obtain a dispersion of 0.16 dex, and in two stars in common with Woolf & Wallerstein (2005), where the [Fe/H] difference for Gl191 and Gl526 is higher than the uncertainties reported here and in their work (0.14 and -0.12 dex, respectively). The offset of each calibration is smaller than the dispersion value of our calibration, aside from Mann et al. (2013b; 0.11 dex). We should note, however, that we only have seven stars in common with Mann et al. (2013b) and one of these stars, Gl205, has a [Fe/H] difference of 0.30 dex. When we consider the full sample we detect a slight increase of dispersion for Rojas-Ayala et al. (2012), and a considerable increase in both dispersion and offset for Newton (2013). This increase in the Newton (2013) dispersion is due to the addition of several stars in common with high [Fe/H], where the two calibrations show most disagreement.

Regarding the effective temperature, the photometric temperature scale of Boyajian et al. (2012) was calculated using the average value of the three colour-metallicity T_{eff} relations ($V - J$, $V - H$, and $V - K_S$) from their Table 9, and imposing a cut-off of $V - K < 4.5$ for the three scales, according to their limits. The T_{eff} values of Woolf & Wallerstein (2005), Rojas-Ayala et al. (2012), Önehag et al. (2012), Mann et al. (2013a), and Rajpurohit et al. (2013a) were taken directly from their works. Figure 14 describes the comparison between our T_{eff} results and those of the other authors. The purple (pointing up) triangles, red crosses, green circles, blue dots, and black (pointing down) triangles correspond to the measurements of Woolf & Wallerstein (2005), Rojas-Ayala et al. (2012), Önehag et al. (2012), Mann et al. (2013a), and Rajpurohit et al. (2013a) respectively. The solid black line in the upper panel defines an identity line. The lower panels show the residuals. The photometric [Fe/H] measurements as well as the T_{eff} determinations using the calibration of Boyajian et al. (2012) were calculated with the data from Table 1.

From Figure 14 and Table 9 we observe a good agreement with the results from Woolf & Wallerstein (2005) where we obtain a low dispersion and offset. However, we only have 5 stars in common with them, and they occupy a very narrow region of the T_{eff} range, around 3500 K. Our results also match well the

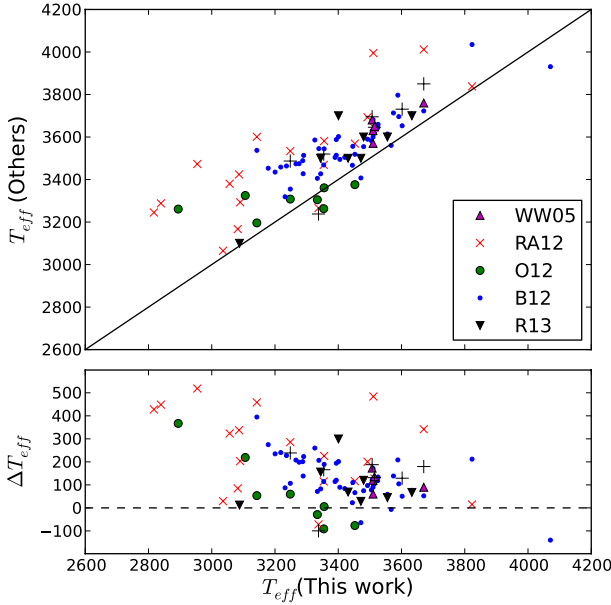


Fig. 14. Upper panel: $T_{\text{eff}}-T_{\text{eff}}$ plot comparing the values of this work, taken from the selected sample, against others in the literature. The solid black line depicts the identity line; lower panel: comparison plot residuals. The dashed black line marks the zero point of our calibration.

Table 10. Linear fit coefficients for each T_{eff} method

T_{eff} method	a	b
Rojas-Ayala et al. (2012)	0.840 ± 0.158	315 ± 555
Önehag et al. (2012)	1.663 ± 1.060	-2250 ± 3499
Mann et al. (2013b)	0.643 ± 0.184	1149 ± 663
Boyajian et al. (2012)	1.079 ± 0.098	-409 ± 349
Rajpurohit et al. (2013a)	0.745 ± 0.171	798 ± 603

BT-SETTL based work of Rajpurohit et al. (2013a). However, when we look at the results of the full sample we observe a significant increase in the rms of Rajpurohit et al. (2013a), and we also witness a considerable dispersion with Rojas-Ayala et al. (2012) in both samples. The Önehag et al. (2012) and Boyajian et al. (2012) determinations tend to converge with ours as the T_{eff} increases. We also note a systematic underestimation of our values of temperature in general that increases below 3200 K. The Önehag et al. (2012) determinations have the smallest offset, but this result is expected since they use the same reference T_{eff} calibration as we do. When we consider the full sample we observe that the rms and offset do not change considerably, except in the case of Rajpurohit et al. (2013a). Finally, we calculated linear fits for the different T_{eff} methods, where $T_{\text{eff}}(\text{This work}) = aT_{\text{eff}}(\text{Others}) + b$. The only exception concerns Woolf & Wallerstein (2005), because the 5 stars we have in common only cover a very narrow range in the effective temperature region. The coefficients a , b and respective uncertainties are reported in Table 10.

4. Discussion

In this paper we present a new high-precision technique to calculate metallicities and effective temperatures for M dwarfs. Within the activity and S/N limits of our method, we achieve a rms of 0.08 dex for metallicity and 91 K for effective temperature. Alternatively we obtain a RMSE_V value of 0.12 dex for [Fe/H] and 293 K for T_{eff} . A bootstrap resampling was also conducted, showing a variation of the rms of [Fe/H] and T_{eff} of

the order of ± 0.01 dex and ± 13 K respectively. Our technique is available for download³. The procedure to use our method is detailed in this webpage as well as in the Annexe. A test of the behaviour of the technique as a function of the resolution and S/N was also performed. We estimate that our method behaves properly down to $R = 40\,000$ and $S/N = 25$, after correcting the observed trends. We also validated our results against a sample of stars in common with SOPHIE high resolution spectra.

To have a measure of the accuracy of our method, we tested it against several studies from the literature. Most studies agree well with our [Fe/H] determinations, and the offset is almost always below the precision of the method. For T_{eff} however, the same agreement could not be met. Despite reaching a good agreement with the results of Woolf & Wallerstein (2005), and Rajpurohit et al. (2013a), that use synthetic spectra from the latest BT-SETTL models, the dispersion as well as the systematics between our determinations and the other works is considerable and beyond the calibration errors. Further studies are needed to investigate the nature of these systematics.

Acknowledgements. We would like to thank Barbara Rojas-Ayala for useful discussions. We would also like to thank Andrew Mann and João Gomes da Silva for kindly providing several metallicity values and the $H\alpha$ determinations, respectively. We acknowledge the support by the European Research Council/European Community under the FP7 through Starting Grant agreement number 239953. The financial support from the “Programme National de Planétologie” (PNP) of CNRS/INSU, France, is also gratefully acknowledged. V.N. acknowledges the support from Fundação para a Ciência e a Tecnologia (FCT) of the fellowship SFRH/BD/60688/2009. N.C.S. also acknowledges the support in the form of a Investigador FCT contract funded by Fundação para a Ciência e a Tecnologia (FCT)/MCTES (Portugal) and POPH/FSE (EC). X.B., T.F. and X.D. would like to acknowledge the support of the French Agence Nationale de la Recherche (ANR), under program ANR-12-BS05-0012 Exo-Atmos. This research has made use of the SIMBAD database, operated at CDS, Strasbourg, France. This publication makes use of data products from the Two Micron All Sky Survey, which is a joint project of the University of Massachusetts and the Infrared Processing and Analysis Center/California Institute of Technology, funded by the National Aeronautics and Space Administration and the National Science Foundation.

Appendix A: Using the method

The code of our technique is written in python 2.7 and can be downloaded at <http://www.astro.up.pt/resources/mcal>. The program is very simple to use. The first step is to write the filenames of your spectra into *stars.txt*, replacing the two demonstration filenames, *G1105B_SID.fits* and *G1849_SID.fits*. Then, one just needs to change the startup options, described in the startup section of the file *runallv1.py*. Depending on the resolution and S/N of the spectra, one should use the values of Table 6 as the reference of precision of [Fe/H] and T_{eff} .

The compressed zip file *calibrationv3.zip* contains all the necessary files needed to run the program, as described in the following list:

- *runallv1.py* – script to run all the other programs. In the startup section one can choose to use fast Fourier transform (FFT) to filter high frequency noise, the file type of the input spectra (FITS or text file), and the name of the file with the full path of the spectra.
- *fft_filterv1.py* – function that performs the FFT filtering of the spectra. The default setting of the filter in *runallv1.py* is “off”.
- *int_calc_stars.py* – function to calculate the pseudo EWs of the relevant lines. It uses *lines.rdb* as input. An output file, *ew_out.npz*, is also created. The function also estimates the

³ <http://www.astro.up.pt/resources/mcal>

$H\alpha$ index described by Gomes da Silva et al. (2011) and warns if the star is too active. It takes 3–5 min per star to calculate the EWs.

- *mcalv1.npz* – function that calculates the $[\text{Fe}/\text{H}]$ and T_{eff} of each star using the calibration matrix file *coef_cal.npz*. The output will be displayed on the screen and can also be optionally saved to a file (check the startup section of *runallv1.py* for details).
- *stars.txt* – text file with the full path of the spectra. This file should have all the spectra files for analysis.
- *G1105B_SID.fits* and *G1849_SID.fits* are two HARPS spectra that can be used to demonstrate how the program works. Their full file names appear in the file *stars.txt*. One should remove them from *stars.txt* before calibrating new stars.

References

- Allard, F., Homeier, D., & Freytag, B. 2011, in 16th Cambridge Workshop on Cool Stars, Stellar Systems, and the Sun, eds. C. Johns-Krull, M. K. Browning, & A. A. West, ASP Conf. Ser., 448, 91
- Allard, F., Homeier, D., & Freytag, B. 2012, Roy. Soc. London Philos. Trans. Ser. A, 370, 2765
- Allard, F., Homeier, D., Freytag, B., et al. 2013, Mem. Soc. Astron. It. Suppl., 24, 128
- Anglada-Escudé, G., Boss, A. P., Weinberger, A. J., et al. 2012, ApJ, 746, 37
- Anglada-Escudé, G., Rojas-Ayala, B., Boss, A. P., Weinberger, A. J., & Lloyd, J. P. 2013, A&A, 551, A48
- Bean, J. L., Sneden, C., Hauschildt, P. H., Johns-Krull, C. M., & Benedict, G. F. 2006, ApJ, 652, 1604
- Blackwell, D. E., & Shallis, M. J. 1977, MNRAS, 180, 177
- Bonfils, X., Delfosse, X., Udry, S., et al. 2005, A&A, 442, 635
- Bonfils, X., Delfosse, X., Udry, S., et al. 2013, A&A, 549, A109
- Bouchy, F., & The Sophie Team. 2006, in Tenth Anniversary of 51 Peg-b: Status of and prospects for hot Jupiter studies, Colloquium held at Observatoire de Haute Provence, France, eds. L. Arnold, F. Bouchy, & C. Moutou, 319
- Boyajian, T. S., von Braun, K., van Belle, G., et al. 2012, ApJ, 757, 112
- Burgasser, A. J., Kirkpatrick, J. D., Reid, I. N., et al. 2003, ApJ, 586, 512
- Casagrande, L., Flynn, C., & Bessell, M. 2008, MNRAS, 389, 585
- Dawson, P. C., & Forbes, D. 1992, AJ, 103, 2063
- Fabrigius, C., Høg, E., Makarov, V. V., et al. 2002, A&A, 384, 180
- Gomes da Silva, J., Santos, N. C., Bonfils, X., et al. 2011, A&A, 534, A30
- Hawley, S. L., Gizis, J. E., & Reid, N. I. 1997, AJ, 113, 1458
- Henden, A. A., Welch, D. L., Terrell, D., & Levine, S. E. 2009, in AAS Meeting Abstracts, 214, 40702
- Henden, A. A., Levine, S. E., Terrell, D., Smith, T. C., & Welch, D. 2012, J. Amer. Association Variable Star Observers (JAAVSO), 40, 430
- Henry, T. J., Jao, W.-C., Subasavage, J. P., et al. 2006, AJ, 132, 2360
- Johnson, J. A., & Apps, K. 2009, ApJ, 699, 933
- Johnson, J. A., Gazak, J. Z., Apps, K., et al. 2012, AJ, 143, 111
- Koen, C., Kilkenny, D., van Wyk, F., & Marang, F. 2010, MNRAS, 403, 1949
- Laing, J. D. 1989, South African Astronomical Observatory Circular, 13, 29
- Leggett, S. K. 1992, ApJS, 82, 351
- Lépine, S., Hilton, E. J., Mann, A. W., et al. 2013, AJ, 145, 102
- Mann, A. W., Brewer, J. M., Gaidos, E., Lépine, S., & Hilton, E. J. 2013a, AJ, 145, 52
- Mann, A. W., Gaidos, E., & Ansdell, M. 2013b, ApJ, 779, 188
- Neves, V., Bonfils, X., Santos, N. C., et al. 2012, A&A, 538, A25
- Neves, V., Bonfils, X., Santos, N. C., et al. 2013, A&A, 551, A36
- Newton, E. 2013, in Protostars and Planets VI, Heidelberg, July 15–20, Poster #1K093, 93
- Önehag, A., Heiter, U., Gustafsson, B., et al. 2012, A&A, 542, A33
- Perryman, M. A. C., Lindgren, L., Kovalevsky, J., et al. 1997, A&A, 323, L49
- Pickles, A. J. 1998, PASP, 110, 863
- Pineda, J. S., Bottom, M., & Johnson, J. A. 2013, ApJ, 767, 28
- Press, W. H., Teukolsky, S. A., Vetterling, W. T., & Flannery, B. P. 1992, Numerical recipes in FORTRAN, The art of scientific computing (Cambridge University Press)
- Rajpurohit, A. S., Reylé, C., Allard, F., et al. 2013a, A&A, 556, A15
- Rajpurohit, A. S., Reylé, C., Schultheis, M., & Allard, F. 2013b, in SF2A-2013: Proc. of the Annual meeting of the French Society of Astronomy and Astrophysics, eds. L. Cambresy, F. Martins, E. Nuss, & A. Palacios, 259
- Reiners, A., Joshi, N., & Goldman, B. 2012, AJ, 143, 93
- Riedel, A. R., Subasavage, J. P., Finch, C. T., et al. 2010, AJ, 140, 897
- Rojas-Ayala, B., Covey, K. R., Muirhead, P. S., & Lloyd, J. P. 2010, ApJ, 720, L113
- Rojas-Ayala, B., Covey, K. R., Muirhead, P. S., & Lloyd, J. P. 2012, ApJ, 748, 93
- Santos, N. C., Israelian, G., & Mayor, M. 2004, A&A, 415, 1153
- Schlaufman, K. C., & Laughlin, G. 2010, A&A, 519, A105
- Ségransan, D., Kervella, P., Forveille, T., & Queloz, D. 2003, A&A, 397, L5
- Skrutskie, M. F., Cutri, R. M., Stiening, R., et al. 2006, AJ, 131, 1163
- Sousa, S. G., Santos, N. C., Israelian, G., Mayor, M., & Monteiro, M. J. P. F. G. 2007, A&A, 469, 783
- Terrien, R. C., Mahadevan, S., Bender, C. F., et al. 2012, ApJ, 747, L38
- Valenti, J. A., Piskunov, N., & Johns-Krull, C. M. 1998, ApJ, 498, 851
- van Leeuwen, F. 2007, A&A, 474, 653
- Weis, E. W. 1993, AJ, 105, 1962
- Weisberg, S. 2005, Applied Linear Regression, Wiley Series in Probability and Statistics (Wiley)
- Wenger, M., Ochsenbein, F., Egret, D., et al. 2000, A&AS, 143, 9
- Woolf, V. M., & Wallerstein, G. 2005, MNRAS, 356, 963
- Woolf, V. M., & Wallerstein, G. 2006, PASP, 118, 218

Table 1. List containing our sample and the quantities used to calculate the reference [Fe/H] and T_{eff} (sorted by right ascension).

Star	$\alpha(2000)$	$\delta(2000)$	π [mas]	π source	Stype (S)	Stype Phot.	V [mag]	J [mag]	H [mag]	Ks [mag]	$V/J/H/K$ source
GI1	00:05:25	-37:21:23	230.4 ± 0.9	H	M1.5	M1.5	8.56 ± 0.02	5.34 ± 0.02	4.73 ± 0.02	4.54 ± 0.02	1/1/1/1
GI54.1	01:12:31	-17:00:00	271.0 ± 8.4	H	M4Ve	M4.0	12.07 ± 0.02	7.26 ± 0.02	6.75 ± 0.03	6.42 ± 0.02	1/8/8/8
GI87	02:12:21	+03:34:30	96.0 ± 1.7	H	M2.5V	M1.5	10.04 ± 0.02	6.83 ± 0.02	6.32 ± 0.03	6.08 ± 0.02	1/8/8/8
GI105B	02:36:16	+06:52:12	139.3 ± 0.5	H	M4.5V	M3.5	11.66 ± 0.02	7.33 ± 0.02	6.79 ± 0.04	6.57 ± 0.02	4/8/8/8
HIP 12961	02:46:43	-23:05:12	43.5 ± 1.7	H	M0	–	10.24 ± 0.02	7.56 ± 0.02	6.93 ± 0.03	6.74 ± 0.02	1/8/8/8
LP771-95A	03:01:51	-16:35:36	146.4 ± 2.9	H06	M3.5	M2.0	10.59 ± 0.05	7.11 ± 0.02	6.56 ± 0.02	6.29 ± 0.02	2/8/8/8
GJ163	04:09:16	-53:22:25	66.7 ± 1.8	H	M3.5	M3.0	11.81 ± 0.02	7.95 ± 0.03	7.43 ± 0.04	7.13 ± 0.02	1/8/8/8
GI176	04:42:56	+18:57:29	106.2 ± 2.5	H	M2	M2.0	9.95 ± 0.02	6.46 ± 0.02	5.82 ± 0.03	5.61 ± 0.03	1/8/8/8
GJ179	04:52:06	+06:28:36	81.4 ± 4.0	H	M3.5	M3.5	12.02 ± 0.04	7.81 ± 0.02	7.21 ± 0.05	6.94 ± 0.02	1/8/8/8
GI191	05:11:40	-45:01:06	255.3 ± 0.9	H	sdM1.0	M0.5	8.85 ± 0.02	5.82 ± 0.03	5.32 ± 0.03	5.05 ± 0.02	1/8/8/8
GI205	05:31:27	-03:40:42	176.8 ± 1.2	H	M1.5V	M1.5	7.97 ± 0.02	4.75 ± 0.05	4.07 ± 0.05	3.85 ± 0.03	1/9/9/9
GI213	05:42:09	+12:29:23	171.6 ± 4.0	H	M4.0V	M4.0	11.56 ± 0.01	7.12 ± 0.02	6.63 ± 0.02	6.39 ± 0.02	3/8/8/8
GI229	06:10:34	-21:51:53	173.8 ± 1.0	H	M1/M2V	M1.0	8.12 ± 0.02	5.06 ± 0.02	4.36 ± 0.02	4.16 ± 0.02	1/1/1/1
HIP 31293	06:33:43	-75:37:47	110.9 ± 2.2	H	M2V	M2.5	10.35 ± 0.01	6.72 ± 0.02	6.15 ± 0.03	5.86 ± 0.02	3/8/8/8
HIP 31292	06:33:47	-75:37:30	114.5 ± 3.2	H	M3V	M3.0	11.41 ± 0.01	7.41 ± 0.03	6.85 ± 0.03	6.56 ± 0.02	3/8/8/8
GI250B	06:52:18	-05:11:24	114.8 ± 0.4	H	M2	M2.0	10.08 ± 0.01	6.58 ± 0.03	5.98 ± 0.06	5.72 ± 0.04	5/8/8/8
GI273	07:27:24	+05:13:30	263.0 ± 1.4	H	M3.5V	M3.5	9.87 ± 0.02	5.71 ± 0.03	5.22 ± 0.06	4.86 ± 0.02	1/8/8/8
GI300	08:12:41	-21:33:12	125.8 ± 1.0	H	M4	M4.0	12.13 ± 0.01	7.60 ± 0.02	6.96 ± 0.03	6.71 ± 0.03	2/8/8/8
GJ2066	08:16:08	+01:18:11	109.6 ± 1.5	H	M2.0V	M2.0	10.09 ± 0.02	6.62 ± 0.03	6.04 ± 0.03	5.77 ± 0.02	1/8/8/8
GJ317	08:40:59	-23:27:23	65.3 ± 0.4	A12	M3.5	M3.0	11.97 ± 0.04	7.93 ± 0.03	7.32 ± 0.07	7.03 ± 0.02	2/8/8/8
GI341	09:21:38	-60:16:53	95.6 ± 0.9	H	M0.0	M0.5	9.46 ± 0.02	6.44 ± 0.02	5.79 ± 0.03	5.59 ± 0.02	1/8/8/8
GJ1125	09:30:44	+00:19:18	103.5 ± 3.9	H	M3.5	M3.0	11.71 ± 0.02	7.70 ± 0.02	7.18 ± 0.03	6.87 ± 0.02	1/8/8/8
GI357	09:36:02	-21:39:42	110.8 ± 1.9	H	M2.5V	M2.5	10.91 ± 0.02	7.34 ± 0.03	6.74 ± 0.03	6.47 ± 0.02	1/8/8/8
GI358	09:39:47	-41:04:00	105.6 ± 1.6	H	M3	M3.0	10.69 ± 0.02	6.90 ± 0.03	6.32 ± 0.05	6.06 ± 0.02	1/8/8/8
GI367	09:44:30	-45:46:36	101.3 ± 3.2	H	M1.0	M1.5	9.98 ± 0.02	6.63 ± 0.02	6.04 ± 0.04	5.78 ± 0.02	1/8/8/8
GI382	10:12:17	-03:44:47	127.1 ± 1.9	H	M2.0V	M2.0	9.26 ± 0.02	5.89 ± 0.02	5.26 ± 0.02	5.01 ± 0.02	1/8/8/8
GI393	10:28:55	+00:50:23	141.5 ± 2.2	H	M2.5V	M2.0	9.63 ± 0.02	6.18 ± 0.02	5.61 ± 0.03	5.31 ± 0.02	1/8/8/8
GJ3634	10:58:35	-31:08:38	50.5 ± 1.6	R10	M2.5	M2.5	11.93 ± 0.02	8.36 ± 0.02	7.76 ± 0.05	7.47 ± 0.03	2/8/8/8
GI413.1	11:09:31	-24:36:00	93.0 ± 1.7	H	M2	M2.0	10.45 ± 0.02	6.95 ± 0.02	6.36 ± 0.04	6.10 ± 0.02	1/8/8/8
GI433	11:35:27	-32:32:23	112.6 ± 1.4	H	M1.5	M1.5	9.81 ± 0.02	6.47 ± 0.02	5.86 ± 0.04	5.62 ± 0.02	1/8/8/8
GI436	11:42:11	+26:42:23	98.6 ± 2.3	H	M3.5V	M2.5	10.61 ± 0.01	6.90 ± 0.02	6.32 ± 0.02	6.07 ± 0.02	2/8/8/8
GI438	11:43:20	-51:50:23	91.7 ± 2.0	R10	M0.0 [†]	M1.5	10.36 ± 0.04	7.14 ± 0.02	6.58 ± 0.04	6.32 ± 0.02	2/8/8/8
GI447	11:47:44	+00:48:16	299.6 ± 2.2	H	M4.5V	M4.0	11.12 ± 0.01	6.50 ± 0.02	5.95 ± 0.02	5.65 ± 0.02	3/8/8/8
GI465	12:24:53	-18:14:30	113.0 ± 2.5	H	M2	M2.0	11.27 ± 0.02	7.73 ± 0.02	7.25 ± 0.02	6.95 ± 0.02	1/8/8/8
GI479	12:37:53	-52:00:06	103.2 ± 2.3	H	M3V(e)	M3.0	10.66 ± 0.02	6.86 ± 0.02	6.29 ± 0.03	6.02 ± 0.02	1/8/8/8
GI514	13:30:00	+10:22:36	130.6 ± 1.1	H	M1.0V	M1.0	9.03 ± 0.02	5.90 ± 0.02	5.30 ± 0.03	5.04 ± 0.03	1/8/8/8
GI526	13:45:44	+14:53:30	185.5 ± 1.1	H	M4.0V	M1.0	8.43 ± 0.02	5.24 ± 0.05	4.65 ± 0.05	4.42 ± 0.02	1/9/9/8
GI536	14:01:03	-02:39:18	98.3 ± 1.6	H	M1.5V	M1.0	9.71 ± 0.02	6.52 ± 0.02	5.93 ± 0.04	5.68 ± 0.02	1/8/8/8
GI555	14:34:17	-12:31:06	165.0 ± 3.3	H	M4.0V	M4.0	11.32 ± 0.02	6.84 ± 0.02	6.26 ± 0.04	5.94 ± 0.03	1/8/8/8
GI569A	14:54:29	+16:06:04	101.9 ± 1.7	H	M2.5V	M3.0	10.41 ± 0.05	6.63 ± 0.02	5.99 ± 0.02	5.77 ± 0.02	6/8/8/8
GI581	15:19:26	-07:43:17	160.9 ± 2.6	H	M5.0V	M3.0	10.57 ± 0.01	6.71 ± 0.03	6.09 ± 0.03	5.84 ± 0.02	3/8/8/8
GI588	15:32:13	-41:16:36	168.7 ± 1.3	H	M2.5V	M2.5	9.31 ± 0.02	5.65 ± 0.02	5.03 ± 0.02	4.76 ± 0.02	1/8/8/8
GI618A	16:20:04	-37:31:41	119.8 ± 2.5	H	M3	M3.0	10.59 ± 0.02	6.79 ± 0.02	6.22 ± 0.02	5.95 ± 0.02	1/8/8/8
GI628	16:30:18	-12:39:47	233.0 ± 1.6	H	M3V	M3.5	10.07 ± 0.02	5.95 ± 0.02	5.37 ± 0.04	5.08 ± 0.02	1/8/8/8
GJ1214	17:15:19	+04:57:50	68.7 ± 0.6	A13	M4.5	M4.0	14.64 ± 0.03	9.75 ± 0.02	9.09 ± 0.02	8.78 ± 0.02	7/8/8/8
GI667C	17:18:58	-34:59:42	146.3 ± 9.0	H	M1.5V	M2.0	10.27 ± 0.04	6.85 ± 0.02	6.32 ± 0.04	6.04 ± 0.02	2/8/8/8
GI674	17:28:40	-46:53:42	220.2 ± 1.4	H	M3V	M2.5	9.41 ± 0.02	5.71 ± 0.02	5.15 ± 0.03	4.86 ± 0.02	1/8/8/8
GJ676A	17:30:11	-51:38:13	60.8 ± 1.6	H	M0V	M0.0	9.59 ± 0.02	6.71 ± 0.02	6.08 ± 0.02	5.83 ± 0.03	1/8/8/8
GI678.1A	17:30:22	+05:32:53	100.2 ± 1.1	H	M1V	M1.0	9.33 ± 0.01	6.24 ± 0.02	5.65 ± 0.04	5.42 ± 0.03	3/8/8/8
GI680	17:35:13	-48:40:53	102.8 ± 2.8	H	M3V	M2.0	10.13 ± 0.02	6.67 ± 0.02	6.08 ± 0.03	5.83 ± 0.02	1/8/8/8
GI682	17:37:03	-44:19:11	196.9 ± 2.1	H	M3.5	M3.5	10.95 ± 0.02	6.54 ± 0.02	5.92 ± 0.04	5.61 ± 0.02	1/8/8/8
GI686	17:37:53	+18:35:30	123.0 ± 1.6	H	M1.0V	M1.5	9.58 ± 0.02	6.36 ± 0.02	5.79 ± 0.02	5.57 ± 0.02	1/8/8/8
GI693	17:46:35	-57:19:11	171.5 ± 2.3	H	M2.0	M3.0	10.78 ± 0.02	6.86 ± 0.02	6.30 ± 0.04	6.02 ± 0.02	1/8/8/8
GI699	17:57:49	+04:41:36	549.0 ± 1.6	H	M4.0V	M3.5	9.51 ± 0.02	5.24 ± 0.02	4.83 ± 0.03	4.52 ± 0.02	1/8/8/8
GI701	18:05:07	-03:01:53	128.9 ± 1.4	H	M2.0V	M1.0	9.36 ± 0.02	6.16 ± 0.02	5.57 ± 0.04	5.31 ± 0.02	1/8/8/8
GI752A	19:16:55	+05:10:05	170.4 ± 1.0	H	M3V B	M2.0	9.12 ± 0.02	5.58 ± 0.03	4.93 ± 0.03	4.67 ± 0.02	1/8/8/8
GI832	21:33:34	-49:00:36	201.9 ± 1.0	H	M1.5	M1.5	8.67 ± 0.02	5.36 ± 0.02	4.69 ± 0.02	4.47 ± 0.02	1/1/1/1
GI846	22:02:10	+01:24:00	97.6 ± 1.5	H	M0	M0.5	9.15 ± 0.02	6.20 ± 0.02	5.56 ± 0.05	5.32 ± 0.02	1/8/8/8
GI849	22:09:40	-04:38:30	109.9 ± 2.1	H	M3.5V	M3.0	10.37 ± 0.02	6.51 ± 0.02	5.90 ± 0.04	5.59 ± 0.02	1/8/8/8
GI876	22:53:17	-14:15:48	213.3 ± 2.1	H	M5.0V	M3.5	10.18 ± 0.02	5.93 ± 0.02	5.35 ± 0.05	5.01 ± 0.02	1/8/8/8
GI877	22:55:46	-75:27:36	116.1 ± 1.2	H	M3V	M2.5	10.38 ± 0.02	6.62 ± 0.02	6.08 ± 0.03	5.81 ± 0.02	1/8/8/8
GI880	22:56:35	+16:33:12	146.1 ± 1.0	H	M2.0V	M1.5	8.64 ± 0.02	5.36 ± 0.02	4.75 ± 0.05	4.52 ± 0.02	1/8/9/9
GI887	23:05:52	-35:51:12	303.9 ± 0.9	H	M2V	M1.0	7.35 ± 0.01	4.17 ± 0.05	3.61 ± 0.05	3.36 ± 0.03	3/9/9/9
GI908	23:49:13	+02:24:06	167.3 ± 1.2	H	M2V	M1.0	8.98 ± 0.01	5.83 ± 0.02	5.28 ± 0.03	5.04 ± 0.02	3/8/8/8
LTT9759	23:53:50	-75:37:53	100.1 ± 1.1	H	Ma	M2.5	10.02 ± 0.02	6.45 ± 0.02	5.78 ± 0.02	5.55 ± 0.03	1/8/8/8

References. H – van Leeuwen (2007); H06 – Henry et al. (2006); A12 – Anglada-Escudé et al. (2012); R10 – Riedel et al. (2010); A13 – Anglada-Escudé et al. (2013); 1 – Koen et al. (2010); 2 – Henden et al. (2009, 2012); 3 – Perryman et al. (1997); 4 – Weis (1993); 5 – Laing (1989); 6 – Fabricius et al. (2002); 7 – Dawson & Forbes (1992); 8 – Skrutskie et al. (2006); 9 – Leggett (1992); S – Simbad; † – Hawley et al. (1997).

Table 2. Our sample table with the reference and calibrated metallicity and effective temperature (sorted by right ascension).

Star	[Fe/H] _{N12} [dex]	[Fe/H] _{NEW} [dex]	T_{effC08} [K]	T_{effNEW} [K]
G11	-0.40	-0.45	3528	3567
G154.1	-0.40	-0.38	2901	3088
G187	-0.30	-0.32	3565	3555
G1105B	-0.14	-0.02	3054	2894
HIP 12961	-0.12	0.22	3904	3823
LP771-95A	-0.51	-0.34	3393	3236
GJ163	0.00	0.07	3223	3276
G1176	0.02	-0.01	3369	3355
GJ179	0.14	0.12	3076	3086
G1191	-0.79	-0.85	3679	3510
G1205	0.17	0.19	3497	3670
G1213	-0.19	-0.11	3026	3082
G1229	-0.04	-0.03	3586	3633
HIP 31293	-0.04	-0.05	3312	3288
HIP 31292	-0.11	-0.06	3158	3184
G1250B	-0.09	-0.08	3369	3453
G1273	-0.05	-0.01	3107	3090
G1300	0.09	0.13	2965	2841
GJ2066	-0.09	-0.17	3388	3421
GJ317	0.22	0.22	3130	3106
G1341	-0.14	-0.14	3633	3575
GJ1125	-0.15	-0.09	3162	3112
G1357	-0.30	-0.30	3335	3344
G1358	0.01	-0.01	3240	3178
G1367	-0.09	-0.07	3452	3394
G1382	0.04	0.02	3429	3401
G1393	-0.13	-0.20	3396	3431
GJ3634	-0.02	-0.07	3332	3405
G1413.1	-0.06	-0.10	3373	3394
G1433	-0.13	-0.17	3450	3480
G1436	0.01	-0.03	3277	3354
G1438	-0.31	-0.36	3536	3505
G1447	-0.23	-0.17	2952	3036
G1465	-0.54	-0.62	3382	3472
G1479	0.05	0.01	3238	3218
G1514	-0.13	-0.16	3574	3526
G1526	-0.18	-0.22	3545	3515
G1536	-0.13	-0.14	3546	3525
G1555	0.13	0.14	2987	2839
G1569A	0.16	-0.06	3235	3289
G1581	-0.18	-0.20	3203	3248
G1588	0.07	0.06	3284	3291
G1618A	-0.05	-0.06	3242	3200
G1628	-0.05	-0.02	3107	3057
GJ1214	0.03	0.05	2856	2817
G1667C	-0.47	-0.50	3431	3445
G1674	-0.18	-0.23	3284	3334
GJ676A	0.10	0.26	3734	4071
G1678.1A	-0.10	-0.14	3611	3591
G1680	-0.07	-0.19	3395	3390
G1682	0.09	0.10	3002	2912
G1686	-0.29	-0.35	3542	3493
G1693	-0.28	-0.28	3188	3232
G1699	-0.59	-0.51	3094	3338
G1701	-0.20	-0.27	3535	3510
G1752A	0.04	0.05	3336	3339
G1832	-0.17	-0.17	3450	3446
G1846	-0.08	0.01	3682	3588
G1849	0.24	0.22	3200	3143
G1876	0.14	0.14	3059	2954
G1877	-0.01	-0.00	3266	3266
G1880	0.05	0.03	3488	3602
G1887	-0.20	-0.24	3560	3507
G1908	-0.38	-0.44	3587	3511
LTT9759	0.17	0.17	3316	3326

Table 4. Full HARPS M dwarf GTO sample (sorted by right ascension).

Star	α (2000) [h]	δ (2000) [deg]	S/N	$\log L_{H\alpha}/L_{\text{bol}}$	$H\alpha(\text{GdS})$	$[\text{Fe}/\text{H}]_{N13}$ [dex]	$[\text{Fe}/\text{H}]$ [dex]	$\sigma[\text{Fe}/\text{H}]$ [dex]	T_{eff} [K]	σT_{eff} [K]
G11	00:05:25	-37:21:23	870	-4.88	0.01	-0.45	-0.45	0.09	3567	110
GJ1002 ¹	00:06:44	-07:32:23	21	-	0.05	-0.19	-0.27	0.20	2718	150
G112	00:15:49	+13:33:17	46	-	0.03	-0.34	-0.29	0.09	3239	110
LHS1134	00:43:26	-41:17:36	35	-	0.03	-0.10	-0.13	0.09	2950	110
G154.1	01:12:31	-17:00:00	107	-4.07	0.18	-0.40	-0.38	0.09	3088	110
L707-74	01:23:18	-12:56:23	33	-	0.03	-0.35	-0.38	0.09	3353	110
G187	02:12:21	+03:34:30	281	-4.88	0.02	-0.31	-0.32	0.09	3555	110
G1105B	02:36:16	+06:52:12	143	-	0.02	-0.02	-0.02	0.09	2894	110
CD-44-836A	02:45:11	-43:44:30	68	-	0.13	-0.08	-0.07	0.09	3032	110
HIP 12961	02:46:43	-23:05:12	384	-	0.07	0.22	0.22	0.09	3823	110
LHS1481	02:58:10	-12:53:06	65	-	0.02	-0.72	-0.76	0.09	3510	110
LP771-95A	03:01:51	-16:35:36	109	-	0.02	-0.34	-0.34	0.09	3236	110
LHS1513 ²	03:11:36	-38:47:17	26	-4.93	0.03	-0.11	-	-	3197	110
GJ1057	03:13:23	+04:46:30	28	-	0.05	0.10	-0.10	0.09	2916	110
G1145	03:32:56	-44:42:06	93	-4.89	0.04	-0.28	-0.28	0.09	3270	110
GJ1061	03:36:00	-44:30:48	28	-	0.07	-0.08	-0.09	0.09	2882	110
GJ1065	03:50:44	-06:05:42	38	-4.93	0.03	-0.22	-0.23	0.09	3062	110
GJ163	04:09:16	-53:22:25	312	-	0.02	0.05	0.07	0.09	3276	110
GJ1068 ¹	04:10:28	-53:36:06	21	-	0.04	-0.30	-0.43	0.20	2887	150
G1166C ¹	04:15:22	-07:39:23	82	-3.95	0.29	0.08	-0.12	0.20	3018	150
G1176	04:42:56	+18:57:29	576	-	0.06	-0.01	-0.01	0.09	3355	110
GJ179	04:52:06	+06:28:36	999	-	0.05	0.11	0.12	0.09	3086	110
LHS1723	05:01:57	-06:56:47	62	-4.51	0.16	-0.25	-0.24	0.09	3167	110
LHS1731	05:03:20	-17:22:23	79	-4.90	0.03	-0.26	-0.19	0.09	3273	110
G1191	05:11:40	-45:01:06	788	-	0.00	-0.88	-0.85	0.09	3510	110
G1203	05:28:00	+09:38:36	68	-4.93	0.03	-0.25	-0.22	0.09	3138	110
G1205	05:31:27	-03:40:42	1430	-4.88	0.09	0.22	0.19	0.09	3670	110
G1213	05:42:09	+12:29:23	105	-4.94	0.01	-0.11	-0.11	0.09	3082	110
G1229	06:10:34	-21:51:53	727	-4.87	0.07	-0.01	-0.03	0.09	3633	110
HIP 31293	06:33:43	-75:37:47	147	-	0.05	-0.04	-0.05	0.09	3288	110
HIP 31292	06:33:47	-75:37:30	125	-	0.04	-0.10	-0.06	0.09	3184	110
G108-21	06:42:11	+03:34:53	56	-	0.03	-0.01	-0.02	0.09	3186	110
G1250B	06:52:18	-05:11:24	167	-	0.05	-0.10	-0.08	0.09	3453	110
G1273	07:27:24	+05:13:30	644	-	0.02	-0.01	-0.01	0.09	3090	110
LHS1935	07:38:41	-21:13:30	77	-4.90	0.03	-0.24	-0.22	0.09	3181	110
G1285 ¹	07:44:40	+03:33:06	85	-3.48	0.90	0.18	0.27	0.20	2946	150
G1299	08:11:57	+08:46:23	69	-4.75	0.04	-0.50	-0.53	0.09	3373	110
G1300	08:12:41	-21:33:12	189	-4.94	0.05	0.14	0.13	0.09	2841	110
GJ2066	08:16:08	+01:18:11	196	-	0.03	-0.18	-0.17	0.09	3421	110
GJ317	08:40:59	-23:27:23	131	-	0.07	0.21	0.22	0.09	3106	110
GJ1123	09:17:05	-77:49:17	28	-	0.04	0.20	0.15	0.09	2779	110
G1341	09:21:38	-60:16:53	471	-	0.05	-0.13	-0.14	0.09	3575	110
GJ1125	09:30:44	+00:19:18	110	-	0.02	-0.11	-0.09	0.09	3112	110
G1357	09:36:02	-21:39:42	258	-	0.01	-0.34	-0.30	0.09	3344	110
G1358	09:39:47	-41:04:00	295	-4.44	0.14	-0.01	-0.01	0.09	3178	110
G1367	09:44:30	-45:46:36	352	-4.88	0.04	-0.07	-0.07	0.09	3394	110
GJ1129	09:44:48	-18:12:48	44	-4.94	0.03	0.07	0.05	0.09	3017	110
G1382	10:12:17	-03:44:47	532	-4.89	0.08	0.04	0.02	0.09	3401	110
G1388 ¹	10:19:36	+19:52:12	589	-3.80	0.40	0.07	0.12	0.20	3171	150
G1393	10:28:55	+00:50:23	464	-4.83	0.04	-0.22	-0.20	0.09	3431	110
LHS288 ¹	10:44:32	-61:11:35	19	-	0.03	-0.60	-0.55	0.20	2760	150
G1402	10:50:52	+06:48:30	70	-	0.04	0.06	0.03	0.09	2943	110
G1406 ¹	10:56:29	+07:00:54	36	-	0.85	0.18	0.19	0.20	2523	150
GJ3634	10:58:35	-31:08:38	204	-	0.03	-0.10	-0.07	0.09	3405	110
G1413.1	11:09:31	-24:36:00	279	-4.88	0.03	-0.12	-0.10	0.09	3394	110
G1433	11:35:27	-32:32:23	599	-	0.03	-0.17	-0.17	0.09	3480	110
G1436	11:42:11	+26:42:23	573	-	0.02	-0.06	-0.03	0.09	3354	110
G1438	11:43:20	-51:50:23	254	-4.82	0.02	-0.39	-0.36	0.09	3505	110
G1447	11:47:44	+00:48:16	133	-	0.03	-0.18	-0.17	0.09	3036	110
G1465	12:24:53	-18:14:30	191	-4.88	0.01	-0.66	-0.62	0.09	3472	110
G1479	12:37:53	-52:00:06	468	-4.88	0.09	0.02	0.01	0.09	3218	110

Notes. ⁽¹⁾ Active star or star with $S/N \leq 25$. The $[\text{Fe}/\text{H}]$ and T_{eff} were calculated using the original photometric calibrations. ⁽²⁾ LHS 1513 is a metal poor star outside the calibration region of [Neves et al. \(2012\)](#). ⁽³⁾ G1 803 is a young, metal rich star outside the calibration region of [Neves et al. \(2012\)](#).

Table 4. continued.

Star	α (2000) [h]	δ (2000) [deg]	S/N	$\log L_{H\alpha}/L_{bol}$	H α (GdS)	[Fe/H] _{N13} [dex]	[Fe/H] [dex]	σ [Fe/H] [dex]	T_{eff} [K]	σT_{eff} [K]
LHS337	12:38:50	-38:22:53	60	-4.97	0.03	-0.25	-0.27	0.09	3007	110
Gl480.1	12:40:46	-43:34:00	77	-	0.03	-0.48	-0.48	0.09	3211	110
Gl486	12:47:57	+09:45:12	70	-	0.02	0.06	0.03	0.09	2941	110
Gl514	13:30:00	+10:22:36	433	-4.91	0.04	-0.16	-0.16	0.09	3526	110
Gl526	13:45:44	+14:53:30	729	-5.02	0.03	-0.20	-0.22	0.09	3515	110
Gl536	14:01:03	-02:39:18	390	-4.88	0.05	-0.12	-0.14	0.09	3525	110
Gl551 ¹	14:29:43	-62:40:47	291	-	0.42	-0.00	0.16	0.20	2654	150
Gl555	14:34:17	-12:31:06	107	-	0.03	0.17	0.14	0.09	2839	110
Gl569A	14:54:29	+16:06:04	182	-4.30	0.23	-0.08	-0.06	0.09	3289	110
Gl581	15:19:26	-07:43:17	773	-	0.01	-0.21	-0.20	0.09	3248	110
Gl588	15:32:13	-41:16:36	602	-4.89	0.03	0.07	0.06	0.09	3291	110
Gl618A	16:20:04	-37:31:41	255	-4.88	0.03	-0.08	-0.06	0.09	3200	110
Gl628	16:30:18	-12:39:47	451	-	0.03	-0.02	-0.02	0.09	3057	110
Gl643	16:55:25	-08:19:23	83	-	0.02	-0.28	-0.26	0.09	3102	110
GJ1214	17:15:19	+04:57:50	999	-	0.04	0.06	0.05	0.09	2817	110
Gl667C	17:18:58	-34:59:42	1025	-4.88	0.02	-0.53	-0.50	0.09	3445	110
Gl674	17:28:40	-46:53:42	686	-4.89	0.06	-0.25	-0.23	0.09	3334	110
GJ676A	17:30:11	-51:38:13	432	-	0.06	0.25	0.26	0.09	4071	110
Gl678.1A	17:30:22	+05:32:53	387	-4.82	0.05	-0.11	-0.14	0.09	3591	110
Gl680	17:35:13	-48:40:53	363	-4.88	0.03	-0.22	-0.19	0.09	3390	110
Gl682	17:37:03	-44:19:11	177	-4.93	0.04	0.11	0.10	0.09	2912	110
Gl686	17:37:53	+18:35:30	328	-	0.02	-0.37	-0.35	0.09	3493	110
Gl693	17:46:35	-57:19:11	133	-	0.03	-0.30	-0.28	0.09	3232	110
Gl699	17:57:49	+04:41:36	496	-	0.01	-0.52	-0.51	0.09	3338	110
Gl701	18:05:07	-03:01:53	520	-	0.04	-0.27	-0.27	0.09	3510	110
GJ1224 ¹	18:07:33	-15:57:47	35	-3.97	0.27	-0.10	-0.25	0.20	2860	150
G141-29 ¹	18:42:44	+13:54:17	24	-	0.26	0.09	-0.08	0.20	3011	150
Gl729 ¹	18:49:49	-23:50:12	135	-3.77	0.31	-0.10	-0.40	0.20	3058	150
GJ1232 ¹	19:09:51	+17:40:07	24	-	0.05	0.14	0.03	0.20	2893	150
Gl752A	19:16:55	+05:10:05	535	-	0.04	0.06	0.05	0.09	3339	110
Gl754	19:20:48	-45:33:30	80	-	0.03	-0.17	-0.14	0.09	3005	110
GJ1236	19:22:03	+07:02:36	53	-	0.03	-0.42	-0.47	0.09	3280	110
GJ1256	20:40:34	+15:29:57	32	-	0.06	0.10	0.06	0.09	2853	110
Gl803 ^{1,3}	20:45:10	-31:20:30	202	-	0.40	0.32	-	-	3430	150
LHS3583	20:46:37	-81:43:12	69	-	0.03	-0.18	-0.22	0.09	3236	110
LP816-60	20:52:33	-16:58:30	97	-	0.04	-0.06	-0.07	0.09	2960	110
Gl832	21:33:34	-49:00:36	925	-	0.03	-0.19	-0.17	0.09	3446	110
Gl846	22:02:10	+01:24:00	643	-4.82	0.07	0.06	0.01	0.09	3588	110
LHS3746	22:02:29	-37:04:54	71	-	0.03	-0.15	-0.13	0.09	3013	110
Gl849	22:09:40	-04:38:30	410	-	0.03	0.24	0.22	0.09	3143	110
GJ1265	22:13:42	-17:41:12	28	-	0.04	-0.09	-0.20	0.09	2941	110
LHS3799 ¹	22:23:07	-17:36:23	25	-	0.36	0.18	0.10	0.20	2820	150
Gl876	22:53:17	-14:15:48	554	-	0.03	0.15	0.14	0.09	2954	110
Gl877	22:55:46	-75:27:36	369	-	0.03	-0.01	-0.00	0.09	3266	110
Gl880	22:56:35	+16:33:12	351	-	0.06	0.07	0.03	0.09	3602	110
Gl887	23:05:52	-35:51:12	1434	-	0.04	-0.24	-0.24	0.09	3507	110
LHS543	23:21:37	+17:17:25	81	-4.94	0.04	0.25	0.23	0.09	2872	110
Gl908	23:49:13	+02:24:06	845	-	0.02	-0.44	-0.44	0.09	3511	110
LTT9759	23:53:50	-75:37:53	168	-	0.07	0.21	0.17	0.09	3326	110

Table 8. Comparison of our parameters with other results from the literature for the stars in common (sorted by right ascension).

Star	Sample	[Fe/H]										T_{eff}												
		This work	B05	SL10	J12	WW05	RA12	O12	T12	EN13	M13a	M13b	This work	WW05	RA12	O12	B12	M13a	M13b	R13				
Gl1	Y	-0.45	-0.52	-0.49	-0.30	-	-	-	-	-	-	-	-	-	-	-	-	-	-	3567	-	3541	-	-
Gl12	N	-0.29	-	-	-	-	-	-	-	-	-	-	-	-	-	-	-	-	-	3239	-	-	-	-
Gl54.1	Y	-0.38	-0.08	-0.49	0.05	-	-	-	-	-	-	-	-	-	-	-	-	-	-	3087	-	-	-	3100
L707-74	N	-0.38	-	-	-	-	-	-	-	-	-	-	-	-	-	-	-	-	-	3352	-	-	-	-
Gl87	Y	-0.32	-0.42	-0.35	-0.52	-	-	-	-	-	-	-	-	-	-	-	-	-	-	3555	-	-	-	3600
Gl105B	Y	-0.02	-0.17	-0.12	-0.26	-	-	-	-	-	-	-	-	-	-	-	-	-	-	2893	-	-	-	-
HIP 12961	Y	0.22	-0.22	-0.10	-0.44	-	-	-	-	-	-	-	-	-	-	-	-	-	-	3823	-	-	-	-
LHS1481	N	-0.76	-	-	-	-	-	-	-	-	-	-	-	-	-	-	-	-	-	3510	-	-	-	-
LP771-95A	Y	-0.34	-0.56	-0.65	-0.17	-	-	-	-	-	-	-	-	-	-	-	-	-	-	3236	-	-	-	-
Gl1057	N	-0.10	-	-	-	-	-	-	-	-	-	-	-	-	-	-	-	-	-	2915	-	-	-	2900
Gl145	N	-0.28	-	-	-	-	-	-	-	-	-	-	-	-	-	-	-	-	-	3269	-	-	-	-
Gl1065	N	-0.23	-	-	-	-	-	-	-	-	-	-	-	-	-	-	-	-	-	3062	-	-	-	3200
Gl163	Y	0.07	-0.06	0.07	-0.13	-	-	-	-	-	-	-	-	-	-	-	-	-	-	3276	-	-	-	-
Gl176	Y	-0.01	-0.03	0.09	-0.05	-	-	-	-	-	-	-	-	-	-	-	-	-	-	3355	-	-	-	-
Gl179	Y	0.12	0.05	0.27	0.14	-	-	-	-	-	-	-	-	-	-	-	-	-	-	3086	-	-	-	-
LHS1723	N	-0.24	-	-	-	-	-	-	-	-	-	-	-	-	-	-	-	-	-	3166	-	-	-	-
LHS1731	N	-0.19	-	-	-	-	-	-	-	-	-	-	-	-	-	-	-	-	-	3272	-	-	-	-
Gl191	Y	-0.85	-0.92	-1.03	-0.50	-	-	-	-	-	-	-	-	-	-	-	-	-	-	3510	-	-	-	-
Gl203	N	-0.22	-	-	-	-	-	-	-	-	-	-	-	-	-	-	-	-	-	3138	-	-	-	-
Gl205	Y	0.19	0.18	0.30	0.07	-	-	-	-	-	-	-	-	-	-	-	-	-	-	3670	-	-	-	3850
Gl213	Y	-0.11	-0.18	-0.20	-0.33	-	-	-	-	-	-	-	-	-	-	-	-	-	-	3082	-	-	-	-
Gl229	Y	-0.03	-0.10	0.01	0.00	-	-	-	-	-	-	-	-	-	-	-	-	-	-	3632	-	-	-	3700
HIP 31293	Y	-0.05	-0.10	0.01	0.01	-	-	-	-	-	-	-	-	-	-	-	-	-	-	3287	-	-	-	-
HIP 31292	Y	-0.06	-0.17	-0.09	0.04	-	-	-	-	-	-	-	-	-	-	-	-	-	-	3183	-	-	-	-
Gl108-21	N	-0.02	-	-	-	-	-	-	-	-	-	-	-	-	-	-	-	-	-	3186	-	-	-	-
Gl250B	Y	-0.08	-0.16	-0.06	-0.04	-	-	-	-	-	-	-	-	-	-	-	-	-	-	3452	-	-	-	-
Gl273	Y	-0.01	-0.12	-0.01	0.08	-	-	-	-	-	-	-	-	-	-	-	-	-	-	3089	-	-	-	-
LHS1935	N	-0.22	-	-	-	-	-	-	-	-	-	-	-	-	-	-	-	-	-	3180	-	-	-	-
Gl299	N	-0.53	-	-	-	-	-	-	-	-	-	-	-	-	-	-	-	-	-	3372	-	-	-	-
Gl300	Y	0.13	-0.02	0.19	0.25	-	-	-	-	-	-	-	-	-	-	-	-	-	-	2840	-	-	-	-
Gl2066	Y	-0.17	-0.15	-0.05	-0.04	-	-	-	-	-	-	-	-	-	-	-	-	-	-	3420	-	-	-	-
Gl317	Y	0.22	0.14	0.36	0.24	-	-	-	-	-	-	-	-	-	-	-	-	-	-	3105	-	-	-	-
Gl1123	N	0.15	-	-	-	-	-	-	-	-	-	-	-	-	-	-	-	-	-	2779	-	-	-	3100
Gl341	Y	-0.14	-0.24	-0.13	-0.18	-	-	-	-	-	-	-	-	-	-	-	-	-	-	3574	-	-	-	-
Gl1125	Y	-0.09	-0.21	-0.14	-0.06	-	-	-	-	-	-	-	-	-	-	-	-	-	-	3111	-	-	-	-
Gl357	Y	-0.30	-0.36	-0.34	-0.01	-	-	-	-	-	-	-	-	-	-	-	-	-	-	3344	-	-	-	3500
Gl358	Y	-0.01	-0.05	0.08	-0.02	-	-	-	-	-	-	-	-	-	-	-	-	-	-	3178	-	-	-	-
Gl367	Y	-0.07	-0.16	-0.07	-0.10	-	-	-	-	-	-	-	-	-	-	-	-	-	-	3393	-	-	-	-
Gl382	Y	0.02	0.00	0.13	-0.01	-	-	-	-	-	-	-	-	-	-	-	-	-	-	3400	-	-	-	3700
Gl393	Y	-0.20	-0.20	-0.11	-0.02	-	-	-	-	-	-	-	-	-	-	-	-	-	-	3431	-	-	-	3500
Gl402	N	0.03	-	-	-	-	-	-	-	-	-	-	-	-	-	-	-	-	-	2943	-	-	-	-
Gl3634	Y	-0.07	-0.08	0.04	0.10	-	-	-	-	-	-	-	-	-	-	-	-	-	-	3404	-	-	-	-
Gl413.1	Y	-0.10	-0.12	-0.02	-0.06	-	-	-	-	-	-	-	-	-	-	-	-	-	-	3393	-	-	-	-

References. B05 – Bonfils et al. (2005); SL10 – Schlafman & Laughlin (2010); J12 – Johnson et al. (2012); WW05 – Woolf & Wallerstein (2005); RA12 – Rojas-Ayala et al. (2012); O12 – Önehan et al. (2012); T12 – Terrien et al. (2012); EN13 – Newton (2013); M13a – Mann et al. (2013a); M13b – Mann et al. (2013b); B12 – Boyajian et al. (2012); R13 – Rajpurohit et al. (2013a).

